JGR

Climatology and variability of trace gases in extratropical double-tropopause regions from MLS, HIRDLS, and ACE-FTS measurements

M. J. Schwartz[1], G. L. Manney[2,3], M. I. Hegglin[4], N. J. Livesey[1], M. L. Santee[1], and W. H. Daffer[1]

[1] Jet Propulsion Laboratory, California Institute of Technology, Pasadena, California, USA, [2] Northwest Research Associates, Socorro, New Mexico, USA, [3] Department of Physics, New Mexico Institute of Mining and Technology, Socorro, New Mexico, USA, [4] Department of Meteorology, University of Reading, Reading, UK

Abstract Upper tropospheric and lower stratospheric measurements from the Aura Microwave Limb Sounder (MLS), the Aura High Resolution Dynamics Limb Sounder (HIRDLS), and the Atmospheric Chemistry Experiment-Fourier transform spectrometer (ACE-FTS) are used to present the first global climatological comparison of extratropical, nonpolar trace gas distributions in double-tropopause (DT) and single-tropopause (ST) regions. Stratospheric tracers, O_3, HNO_3, and HCl, have lower mixing ratios ~2–8 km above the primary (lowermost) tropopause in DT than in ST regions in all seasons, with maximum Northern Hemisphere (NH) differences near 50% in winter and 30% in summer. Southern Hemisphere winter differences are somewhat smaller, but summer differences are similar in the two hemispheres. H_2O in DT regions of both hemispheres shows strong negative anomalies in November through February and positive anomalies in July through October, reflecting the strong seasonal cycle in H_2O near the tropical tropopause. CO and other tropospheric tracers examined have higher DT than ST values 2–7 km above the primary tropopause, with the largest differences in winter. Large DT-ST differences extend to high NH latitudes in fall and winter, with longitudinal maxima in regions associated with enhanced wave activity and subtropical jet variations. Results for O_3 and HNO_3 agree closely between MLS and HIRDLS, and differences from ACE-FTS are consistent with its sparse and irregular midlatitude sampling. Consistent signatures in climatological trace gas fields provide strong evidence that transport from the tropical upper troposphere into the layer between double tropopauses is an important pathway for stratosphere-troposphere exchange.

1. Introduction

Many uncertainties remain regarding the composition of the extratropical upper troposphere/lower stratosphere (UTLS), the processes controlling it, its expected evolution in a changing climate, and its representation in data assimilation systems (DASs) and climate models [see, e.g., *Gettelman et al.*, 2011, and references therein]. Both radiative forcing and surface temperature have their greatest sensitivities to ozone (O_3) and water vapor (H_2O) changes near the tropopause [e.g., *Forster and Shine*, 1997; *Solomon et al.*, 2010]. Transport processes in the UTLS are closely linked to the tropopause and the UTLS jets, which are themselves sensitive to climate change and O_3 depletion [e.g., *Seidel and Randel*, 2006; *Lorenz and DeWeaver*, 2007; *Son et al.*, 2008; *McLandress et al.*, 2011; *World Meteorological Organization*, 2011; *Grise et al.*, 2013].

The abrupt drop in the height of the primary (lowest-altitude) thermal tropopause (the "tropopause break"), from ~16–18 km on the equatorward side of the subtropical upper tropospheric jet (STJ) to below 13 km on the poleward side of the STJ, is a key climatological feature related to extratropical stratosphere-troposphere exchange (STE) [*Holton et al.*, 1995; *Stohl et al.*, 2003, and references therein]. Multiple thermal tropopauses, usually occurring poleward of the tropopause break, have been reported since the early studies of temperature soundings [e.g., *Bjerknes and Palmen*, 1937; *Kochanski*, 1955]. Recent studies have demonstrated that they are common in both hemispheres throughout the year and often occur when the high-altitude tropical tropopause extends poleward across the top of the STJ and over the lower extratropical tropopause [e.g., *Schmidt et al.*, 2006; *Seidel and Randel*, 2006; *Añel et al.*, 2007; *Randel et al.*, 2007a; *Castanheira et al.*, 2009; *Manney et al.*, 2014].

The climatology of multiple tropopauses (MTs) has been examined in high-resolution radiosonde data [e.g., *Seidel and Randel*, 2006; *Añel et al.*, 2008], in Global Positioning System satellite data [e.g., *Schmidt et al.*, 2006; *Randel et al.*, 2007a], and in Aura High Resolution Dynamics Limb Sounder (HIRDLS) data

[*Peevey et al.*, 2012]. A "tropopause inversion layer" (TIL) [e.g., *Birner et al.*, 2006] of enhanced static stability (N^2) often occurs just above the primary tropopause in the same regions and seasons as MTs [e.g., *Randel et al.*, 2007b; *Grise et al.*, 2010]. *Wang and Polvani* [2011] showed that MTs form across an upper tropospheric jet in idealized baroclinic life cycle experiments only when there is a sufficiently strong TIL; in their experiments, MTs formed predominantly in regions of upper level cyclonic flow, consistent with observations [e.g., *Randel et al.*, 2007a]. *Peevey et al.* [2014] showed that extratropical double-tropopause frequencies increase with increasing TIL strength and showed evidence of warm conveyor belts as a mechanism for this relationship. MTs are also common in regions of Rossby wave breaking [e.g., *Pan et al.*, 2009; *Homeyer and Bowman*, 2013]. *Manney et al.* [2014] discuss concurrent seasonal, longitudinal, and hemispheric variations of jet and MT occurrence in a climatology from a meteorological reanalysis data set, showing that extratropical MTs are strongly correlated with greater jet occurrence frequencies and form preferentially in regions with nonzonal jet structure, where they follow the latitudinal variability in the jets, supporting previous results showing more frequent MTs in regions of enhanced synoptic activity [e.g., *Añel et al.*, 2008]. *Homeyer and Bowman* [2013] showed that Rossby wave breaking is an important mechanism for rapid two-way exchange of air between the tropical UTLS and the extratropical lower stratosphere, with the transport direction depending primarily on the positions of the upper tropospheric jets.

Case studies have associated extratropical MTs with intrusions of tropospheric air into the lowermost stratosphere (LMS) [e.g., *Pan et al.*, 2009; *Homeyer et al.*, 2011]. Transport in multiple-tropopause regions is thus expected to be an important factor in extratropical STE and hence in determining the composition of the UTLS. Several recent studies show cases where low-latitude air from the tropical tropopause layer (TTL) [e.g., *Fueglistaler et al.*, 2009] is transported poleward into the extratropical LMS. *Randel et al.* [2007a] showed Stratospheric Aerosol and Gas Experiment II ozone profiles that suggested differences between ozone distributions in MT and single-tropopause (ST) regions. *Pan et al.* [2009] used HIRDLS ozone data, along with ozonesondes and meteorological analyses, in a case study of an intrusion of low-ozone tropical air into a MT region. Intrusions of tropospheric air into MT regions also have been reported in START08 aircraft campaign data [e.g., *Homeyer et al.*, 2011]. *Castanheira et al.* [2012] present a statistical analysis of relationships between the upward branch of the Brewer-Dobson circulation, the area covered by double tropopauses (DTs), and stratospheric O_3 and lower stratospheric H_2O. While their statistical results cannot provide direct information on transport pathways, they show correlations between column O_3, O_3 laminae, wave activity, and areas of DTs that are consistent with those expected from tropical to extratropical transport in the UTLS. *Homeyer et al.* [2014] show that DTs are also preferred regions for convective injection of high H_2O into the stratosphere and argue that reduced stability associated with DTs may facilitate deeper levels of convective overshooting.

By contrast, the theoretical study of *Wang and Polvani* [2011] found that the air between DTs was primarily from high latitudes. Lagrangian transport calculations of *Añel et al.* [2012] also indicate that much of the air between MTs originated in middle to high latitudes. Intrusions of stratospheric air into the troposphere in "tropopause folds" [e.g., *Danielsen*, 1968; *Shapiro*, 1980] often occur in the region just poleward of the STJ [*Holton et al.*, 1995, and references therein], where MTs are common and thus may influence atmospheric composition in their vicinity. The case studies of *Vogel et al.* [2011] indicated that tropospheric intrusions observed by aircraft between DTs originated primarily in the TTL but that stratospheric intrusions (of middle-/high-latitude origin) into the same region could approximately balance their effect on mean composition. *Ungermann et al.* [2013] showed a case study where tropical and subtropical upper tropospheric air and air from both the lowermost and the overlying stratosphere advected into a MT region during a Rossby wave breaking event led to a complex filamentary trace gas structure in that region. These studies indicate several potential pathways for transport into MT regions, each expected to have a different trace gas signature.

Given the ubiquity of MT regions, knowledge of the trace gas distributions associated with them not only is important in assessing the roles of various transport pathways but also is critical to developing a comprehensive picture of the composition of the extratropical UTLS and the radiative impacts of trace gas variability/changes in this region. Previous studies of trace gas distributions in MT regions have presented case studies and some statistical relationships, but no detailed examination of the global climatology has been done. Several high-quality, global, multiyear satellite data sets are now available that are suited to developing this type of climatology. Here we use data sets described by *Manney et al.* [2011] that associate dynamical fields derived from DAS, including tropopause and UTLS jet locations, with satellite-based

composition measurements from the Aura Microwave Limb Sounder (MLS), HIRDLS, and the Atmospheric Chemistry Experiment-Fourier Transform Spectrometer (ACE-FTS) instruments to develop and compare climatologies of trace gas distributions in extratropical regions with single and multiple tropopauses. The three satellite data sets used here each have strengths and weaknesses in terms of their temporal and spatial coverage, sampling patterns, resolution, species measured, and data precision and accuracy; therefore, evaluation of the consistency of results from these data sets provides valuable information to guide further UTLS studies.

Section 2.1 describes the satellite and DAS data sets that are used in this work. Section 2.2 shows the climatology of MTs, and associated dynamical structure from the jet/tropopause catalog, illuminating the dynamical conditions under which MTs occur. Section 2.3 compares the seasonally varying latitudinal sampling of extratropical DT regions by the three satellites used. In section 3.1, we present March Northern Hemisphere climatologies of atmospheric constituent profiles from MLS, HIRDLS, and ACE-FTS in MT regions, along with temperature and potential vorticity (PV) from the DAS, as an example showing the typical vertical distributions of trace gases. A climatology of the seasonal and hemispheric variability of trace gases in single- and double-tropopause profiles is presented in section 3.2, along with discussion of the consistency among these data sets and implications of their different sampling of MT regions. A summary and conclusions are given in section 4.

2. Data and Analysis

2.1. Data Description

MLS [*Waters et al.*, 2006], launched on the Aura satellite in July 2004, measures thermal emission from the Earth's atmospheric limb (viewed along tangent paths) near atmospheric spectral lines between 118 GHz and 2.5 THz. MLS views forward along the orbital path, making 240 vertical scans of the limb per orbit. From these radiances, ~3500 profiles per day are retrieved of temperature, cloud ice, and more than 15 atmospheric gas phase constituents including O_3 [*Livesey et al.*, 2008], H_2O [*Read et al.*, 2007], nitric acid (HNO_3) [*Santee et al.*, 2007], hydrochloric acid (HCl) [*Froidevaux et al.*, 2008], and carbon monoxide (CO) [*Livesey et al.*, 2008]. Version 3 (v3) of these five gas phase products from 2005 to 2012 is used in this work, screened per recommendations of the MLS v3 data quality document [*Livesey et al.*, 2013]. HCl at 147 hPa has a high bias at low latitudes, and this level is generally not recommended for scientific use, but *Santee et al.* [2011] have demonstrated its utility outside of the tropics, and it has been included in this analysis. Vertical resolutions of these products in the tropopause region are ~3 km for O_3 and HCl, ~3.5 km for HNO_3, 4.5 km for CO, and 2.5–3 km for H_2O, and previous work [e.g., *Manney et al.*, 2009, 2011; *Schwartz et al.*, 2013] indicates that useful signatures of variation are captured at somewhat finer vertical scales than these nominal resolutions. Precisions of these products are typically several times smaller (better) than the typical variability of the mixing ratios (the signal), and monthly MLS ST and MT ensembles typically include more than 40,000 measurements, so the impact of single-measurement precision on monthly averages is negligible. Estimated accuracies at the pressure levels of interest in this work are ~0.2 ppmv and 5% for O_3, ~10% for H_2O, ~1 ppbv and 10% for HNO_3, ~0.2 ppbv and 10–100% for HCl, and ~50% for CO [*Livesey et al.*, 2013].

HIRDLS [*Gille et al.*, 2003], also on Aura, measures infrared thermal emission from the Earth's atmospheric limb. Despite the obstruction of most of the HIRDLS limb viewing port [*Gille et al.*, 2005], HIRDLS produced scientifically useful data from January 2005 until 17 March 2008. In this work we use HIRDLS version 07.00 (v7) O_3, HNO_3, H_2O, CFC-11 (CCl_3F), and CFC-12 (CCl_2F_2) from January 2005 to March 2008. These data are described in and screened per the recommendations of the HIRDLS v7 data quality document [*Gille and Gray*, 2013]. Previous versions of O_3 and HNO_3 are described and validated in *Nardi et al.* [2008] and *Kinnison et al.* [2008], respectively. HIRDLS O_3 has 1 km vertical resolution at and above 12 km altitude, with precision of 3–5% and accuracy of 5–10% estimated from correlative measurements. HIRDLS HNO_3 has ~1 km vertical resolution down to 11 km and a precision of 0.1–1 ppbv, degrading with height. The HIRDLS H_2O product, newly available in v7, has a vertical resolution at midlatitudes of 1 km down to ~10 km altitude, increasing to 2 km at 7–8 km.

ACE-FTS [*Bernath et al.*, 2005], launched on Canada's SCISAT-1 satellite in August 2003, views the Sun through the Earth's atmosphere during one "sunrise" and one "sunset" on each orbit, and these solar occultations provide profiles of temperature, pressure, and over 30 chemical species, from the upper troposphere into the mesosphere. ACE version 3 atmospheric constituent measurements [*Boone et al.*, 2013] from the

years 2004–2010 used in this work are newer versions of generally similar but more extensively validated version 2 products [*Boone et al.*, 2005], O_3 [*Dupuy et al.*, 2009; *Hegglin et al.*, 2008], H_2O [*Hegglin et al.*, 2008], HNO_3 [*Kerzenmacher et al.*, 2005; *Wolff et al.*, 2008], CO [*Clerbaux et al.*, 2008; *Hegglin et al.*, 2008], and HCl [*Mahieu et al.*, 2008]. These products have stated vertical resolutions of 3–4 km, which corresponds to the vertical width of the instrument field of view. *Hegglin et al.* [2008] have shown that ACE-FTS retrievals of O_3, H_2O, and CO in the UTLS can achieve near 1 km vertical resolution by exploiting vertical oversampling relative to this field of view width.

ACE-FTS makes, at most, two solar occultation measurements per orbit, and the orbital orientation was chosen to concentrate occultations at high latitudes. Sunrises and sunsets pass briefly through low- and middle latitudes only once every 2 months (e.g., ~3 days of 61 at latitudes 30°S–30°N), so while the precision of individual measurements is generally excellent, sampling of latitudes of interest in this study is sparse and biased to the higher latitudes of that region.

In this work we use temperatures and other dynamical fields from the NASA Global Modeling and Assimilation Office (GMAO) Goddard Earth Observing System (GEOS) version 5 [*Rienecker et al.*, 2008] to produce a consistent set of meteorological fields. GEOS-5-based dynamical and thermal tropopauses (including MTs) and UTLS jet characteristics are routinely cataloged both on the native GEOS-5 grid and at MLS, ACE-FTS, and HIRDLS measurement locations, as described by *Manney et al.* [2011]. Dynamical quantities, including PV, temperature, winds, N^2, lapse rate, and others, are also cataloged, both at the jet and tropopause locations and at the satellite measurement locations. Operational versions of near real-time GEOS-5 data products (GEOS-5.1 before September 2008 and GEOS-5.2 after that) used in this processing have generally consistent UTLS fields of interest (pressure, temperature, geopotential height, horizontal winds, and PV).

2.2. Double-Tropopause Definitions and Distributions

Using the *World Meteorological Organization* [1957] (WMO) definition, thermal tropopauses are identified at any point in a GEOS-5 temperature profile up to the 15 hPa pressure level (~25 km) where the temperature lapse rate falls below 2 K/km and remains below this value, on average, for at least 2 km. The lowest-altitude tropopause thus identified is designated the "primary" tropopause. Additional tropopauses are identified higher in the profile where the lapse rate, after again exceeding 2 K/km, drops below 2 K/km and remains below this value, on average, for another 2 km; they are successively labeled "secondary," "tertiary," etc., with increasing height. Temperature lapse rates are calculated on the native GEOS-5 grid and are vertically interpolated to identify the heights meeting the WMO tropopause criteria. Hereinafter, "tropopause" will refer to a thermal tropopause meeting the WMO definition, unless further qualified. The primary (secondary) thermal tropopause is referred to hereinafter as Tp1 (Tp2). Single- (double-)tropopause regions/profiles are denoted as ST (DT).

Analysis in this work is confined to ST and DT profiles, with profiles of higher multiplicities excluded. In every season and hemisphere, triple-tropopause profiles (3xTp) make up less than 2% of MTs, and they make up less than 0.5% of MTs in the global distribution, so their inclusion or exclusion does not significantly alter our results. Furthermore, in winter, when they are most prevalent, we have found 3xTp profiles often to be associated with the temperature structure of the polar vortex (not shown). Indeed, the highest fractions of 3xTPs in records from a variety of radiosonde sites shown by *Randel et al.* [2007a] were in winter profiles from an Alaskan site, consistent with this connection of 3xTPs to polar winter dynamics. Exclusion of 3xTp profiles helps maintain the desired focus on the distinct dynamical regime associated with the tropical boundary. The misidentification of low-altitude inversions as Tp1s can also lead to the inclusion of truly tropospheric air in stratospheric averages when profiles are aligned by Tp1, misalignment that is particularly problematic for species such as H_2O that have extremely strong gradients at Tp1. Profiles with more than two tropopauses have a high incidence of these false Tp1s, so their exclusion from these analyses is prudent.

The "dynamical tropopause" is associated with the sharp increase in PV at the top of the extratropical troposphere. The 3.5×10^{-6} m^2 s^{-1} K kg^{-1} (3.5 pvu) contour of PV defines one such dynamical tropopause ($TpD_{3.5}$) that generally corresponds closely to the primary thermal tropopause in midlatitudes [e.g., *Hoinka*, 1998; *Schoeberl*, 2004]. The height of this PV surface will be used as a criterion for distinguishing tropical from extratropical profiles. PV inversions that result in a secondary $TpD_{3.5}$ are extremely rare (<0.05% of profiles) in the GEOS-5 PV record. *Kunz et al.* [2011] have shown that the value of PV associated with the tropopause transport barrier is an increasing function of potential temperature (θ), so a dynamic tropopause defined at a θ-dependent PV might provide MTs more consistent with those from the WMO thermal tropopauses.
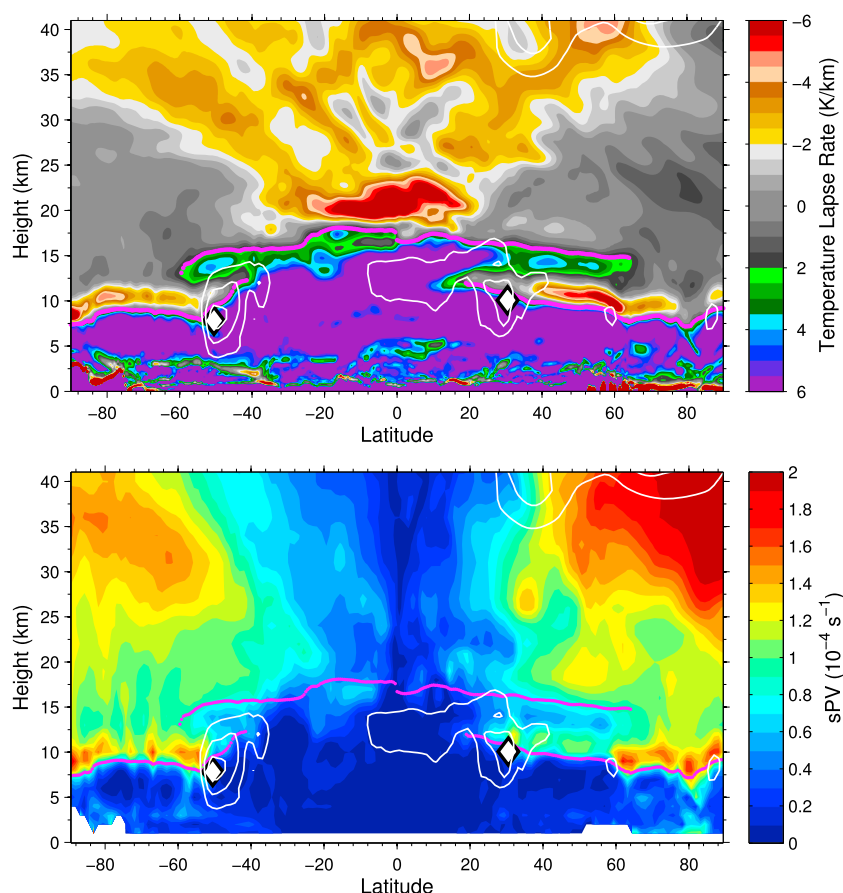
Figure 1. (top) GEOS-5 temperature lapse rate and (bottom) scaled potential vorticity for 125°W on 1 March 2006. The WMO tropopause is marked in magenta. STJ cores are marked with black-outlined white diamonds, and jet wind contours (white lines) are in steps of 10 m/s from the outermost contour at 30 m/s.

In this work we use $TpD_{3.5}$ only as an additional tool to reject tropical profiles, and, for this purpose, the fixed 3.5 pvu definition is sufficient.

Figure 1 (top) shows an example of GEOS-5 temperature lapse rates, with overlaid tropopause and upper tropospheric jet locations in a meridional cross section at 125°W on 1 March 2006, a representative day with extensive DTs. By definition, WMO tropopauses (magenta lines) are at the green-gray (2 K/km) lapse rate transition. Upper tropospheric jet cores are identified as each latitude/altitude point in a fixed-longitude slice where the local maximum wind speed exceeds 40 m s^{-1}, with the boundaries of the jet regions defined by the surrounding 30 m s^{-1} wind speed contour (additional criteria are applied to determine whether two maxima within the same jet region are counted separately [*Manney et al.*, 2011]). For the meridional slice shown, the high tropical WMO tropopause extends over the STJ in both hemispheres, forming a secondary tropopause about 5 km above the primary extratropical WMO tropopause. In both hemispheres, the primary and secondary extratropical tropopauses generally decrease in height with increasing latitude. Resulting nearly parallel tropopauses, particularly evident in the NH of Figure 1, often characterize DT regions [e.g., *Randel et al.*, 2007a; *Añel et al.*, 2008]. In the NH, the secondary tropopause extends from 20° to 65°N latitude, resulting in an unusually extensive DT region of 45° in latitude. The maximum in N^2 in the TIL just above the primary tropopause [e.g., *Birner et al.*, 2006; *Grise et al.*, 2010] is associated with the large negative lapse rates that are evident in the tropics, at high southern latitudes and along ~40–60°N; the appearance of a TIL in these regions during this season is consistent with climatological results [e.g., *Grise et al.*, 2010; *Randel and Wu*, 2010].

PV, which is the product of absolute vorticity and N^2, is useful for identifying air mass origins, as it is conserved on isentropic surfaces in the absence of diabatic and frictional processes [e.g., *Hoskins et al.*, 1985; *Ertel*, 1942]. PV may be scaled in "vorticity units" [*Dunkerton and Delisi*, 1986] by dividing by a single standard
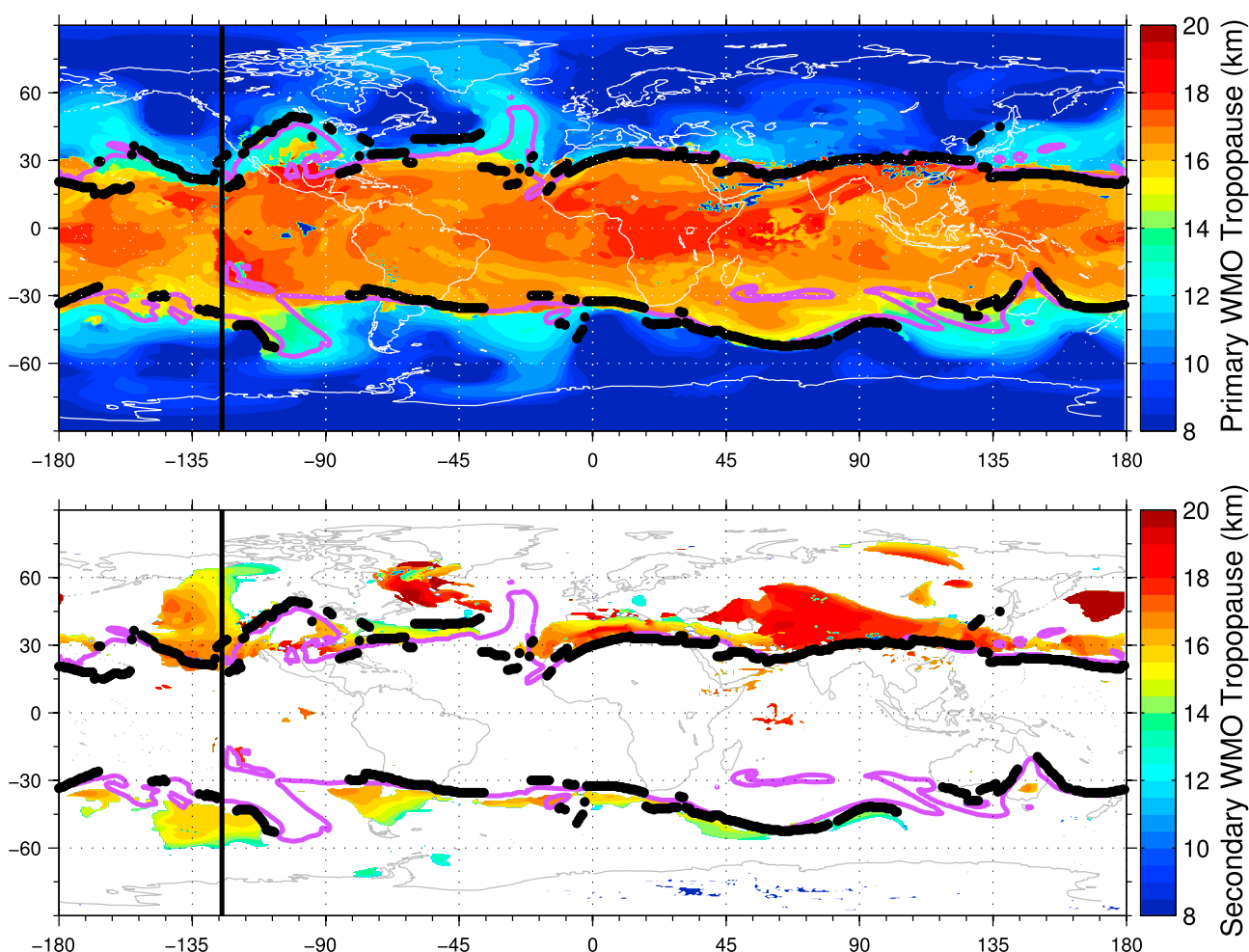
Figure 2. Maps showing (top) primary and (bottom) secondary WMO tropopause altitudes, derived from GEOS-5 reanalysis (MERRA), for 1 March 2006, 0 UTC. Identified subtropical jet cores are marked with black dots. The 13 km contour of $TpD_{3.5}$ is indicated with a magenta line. The 125°W meridian shown in Figure 1 is indicated in black.

atmosphere value of $d\theta/dz$ characteristic of the stratosphere at each potential temperature level. The resulting "scaled" PV (sPV) has a similar range of values throughout the stratosphere but drops abruptly near the tropopause because of the large change in the actual N^2 there. Since extratropical sPV is uniformly positive in the NH and negative in the SH, hereinafter "sPV" will refer to and will be shown as an unsigned quantity, facilitating comparisons of the hemispheres in discussions and the use of common color tables in figures. Tropospheric and low-latitude air has low sPV, typically $< 0.2 \times 10^{-4} \, s^{-1}$, and stratospheric middle- and high-latitude air has higher values, typically $> 0.8 \times 10^{-4} \, s^{-1}$. The sPV at the stratospheric polar vortex edge is typically near $1.4 \times 10^{-4} \, s^{-1}$ [e.g., *Manney et al.*, 1994, 2007].

Figure 1 (bottom) shows sPV for the same latitudinal cross section as is shown in Figure 1 (top), with the same wind speed contours, jet cores, and WMO tropopauses overlaid. In the regions where DTs exist, the ~3 km layer just below Tp2 contains air with low sPV values, suggesting low-latitude and/or tropospheric origins. The high N^2 of the TIL is associated with higher values of sPV. The relationships of sPV, lapse rates, and thermal tropopauses seen in this example are similar to those shown by *Pan et al.* [2009] in a case study of a tropospheric intrusion associated with a DT region.

Figure 2 shows the global distribution of Tp1 (top) and Tp2 (bottom) heights, again for 1 March 2006. The 125°W meridian that was shown in Figure 1 is indicated in black. Our focus in this study is the comparison of composition in extratropical, nonpolar ST and DT regions, where the DTs are extensions of the high tropical tropopause poleward over the STJ as shown in Figure 1. The STJ, at longitudes where it exists, is identified as the lowest-latitude westerly jet in each hemisphere for which $TpD_{3.5}$ is higher than 14 km on

the equatorward jet boundary and drops by more than 2 km from the equatorward boundary to the poleward boundary of the jet. STJ cores (black dots) and the 13 km contour of $TpD_{3.5}$ (magenta line) are generally quite close to one another and either might be used as a latitudinal threshold to exclude "tropical" profiles from our analysis, but the 13 km primary $TpD_{3.5}$ threshold is preferred because it can be used at longitudes where there is no jet. The dynamical tropopause is preferred for this purpose to the WMO tropopause, Tp1, both because it is physically linked to transport characteristics [e.g., *Holton et al.*, 1995; *Bethan et al.*, 1996; *Highwood et al.*, 2000] and because it avoids the problem of spurious low-altitude thermal tropopauses that can result from tropospheric temperature inversions. The extratropical screening used in this work (criteria enumerated below) rejects profiles with either $TpD_{3.5}$ or Tp1 above 13 km, with the additional Tp1 criteria eliminating occasional very low latitude, high-PV pockets of air from the extratropical ensemble.

Figure 2 (bottom) shows that there are double WMO tropopauses on the poleward side of the STJ at many longitudes in both hemispheres and that they are particularly extensive in the Northern (winter) Hemisphere. The tongue of double tropopauses along the west coast of North America that descends slightly with increasing latitude beyond 60°N contains the 125°W meridional slice shown in Figure 1. Over the next 6 days (not shown), this region of DTs extends poleward beyond 80°N over North America and interacts with the weak lower stratospheric polar vortex that has reformed after a sudden stratospheric warming event earlier in the season.

While not seen in the weak polar vortex conditions on 1 March 2006, it is common for the polar night stratosphere to have a volume of low temperatures, the bottom edge of which meets the definition of a WMO tropopause at 18–25 km [e.g., *Bethan et al.*, 1996; *Zängl and Hoinka*, 2001; *Wilcox et al.*, 2012; *Manney et al.*, 2014]. As is discussed in detail by *Manney et al.* [2014], these DT profiles are phenomenologically different than those of interest in this work, which are extensions of the tropical tropopause over the STJ and which typically are below 19 km at their tropical edge (near the STJ) and decrease in altitude toward the pole.

The criteria that we will use to select "extratropical" (by which, hereinafter, we always mean "extratropical, nonpolar") profiles exclude the following: (1) profiles with more than two (WMO) tropopauses, (2) profiles with Tp1 < 5.5 km, (3) profiles with Tp1 > 13 km, (4) profiles with $TpD_{3.5}$ > 13 km, (5) profiles poleward of 60°, (6) profiles with sPV > 1.2×10^{-4} s^{-1} at 46 hPa (21 km), (7) profiles with sPV > 1.4×10^{-4} s^{-1} at 10 hPa (32 km), and (8) profiles with Tp2 > 20 km.

The first screening criterion avoids misidentified tropopauses and polar vortex-influenced profiles that are beyond the scope of the current work. Criterion 2 removes profiles that have low-altitude temperature inversions. Criteria 3 and 4 conservatively avoid tropical profiles. Criterion 5 restricts the study to the midlatitude extratropics. Criteria 6 and 7 avoid profiles within the polar vortex. Criterion 8 excludes profiles with Tp2 greater than 20 km, which are also often associated with polar vortex temperature structure [*Manney et al.*, 2014, and references therein]. Although the distinction between polar and nonpolar DTs is sometimes blurred, particularly over the North Atlantic and Europe when the polar vortex is shifted over these regions (see examples and discussion in *Manney et al.* [2014]), the combined altitude/sPV/latitude screening described here is reasonably effective in eliminating from our analyses DTs that are primarily associated with the polar winter vortex.

Figure 3 shows bimonthly climatologies of extratropical (screened as described above) DT occurrence frequencies (DT%) based on GEOS-5 WMO tropopauses at MLS observation locations for 2005–2012 (the years for which we use MLS data and a superset of those years for which we use HIRDLS and ACE-FTS data). The overall features in these maps agree well with those in the 34 year seasonal climatology of MTs in relation to UTLS jets shown by *Manney et al.* [2014], except here we have removed polar DTs. *Peevey et al.* [2012] showed substantial interannual variability in DT frequencies during the 4 years sampled by HIRDLS. Further evidence for significant interannual variability was given by *Manney et al.* [2014], who showed that differences in the climatological patterns of DT occurrence between HIRDLS and the 34 year Modern-Era Retrospective Analysis for Research and Applications (MERRA) reanalysis resulted primarily from the different time periods considered. However, in the analyses below, it is found that limiting MLS observations to the HIRDLS period (not shown) has only very minor impacts on observed differences between DT and ST climatologies. The high rates of DTs along the STJ in winter/spring, particularly in the Northern Hemisphere (NH), and the high rate of DTs on the poleward edges of the NH summer monsoon regions are characteristics of the long-term climatology. Along the poleward edge of the winter STJ, DT fractions are 30–65% in the NH and 20–50% in the Southern Hemisphere (SH). High DT fractions are also seen in summer along the STJ poleward of the
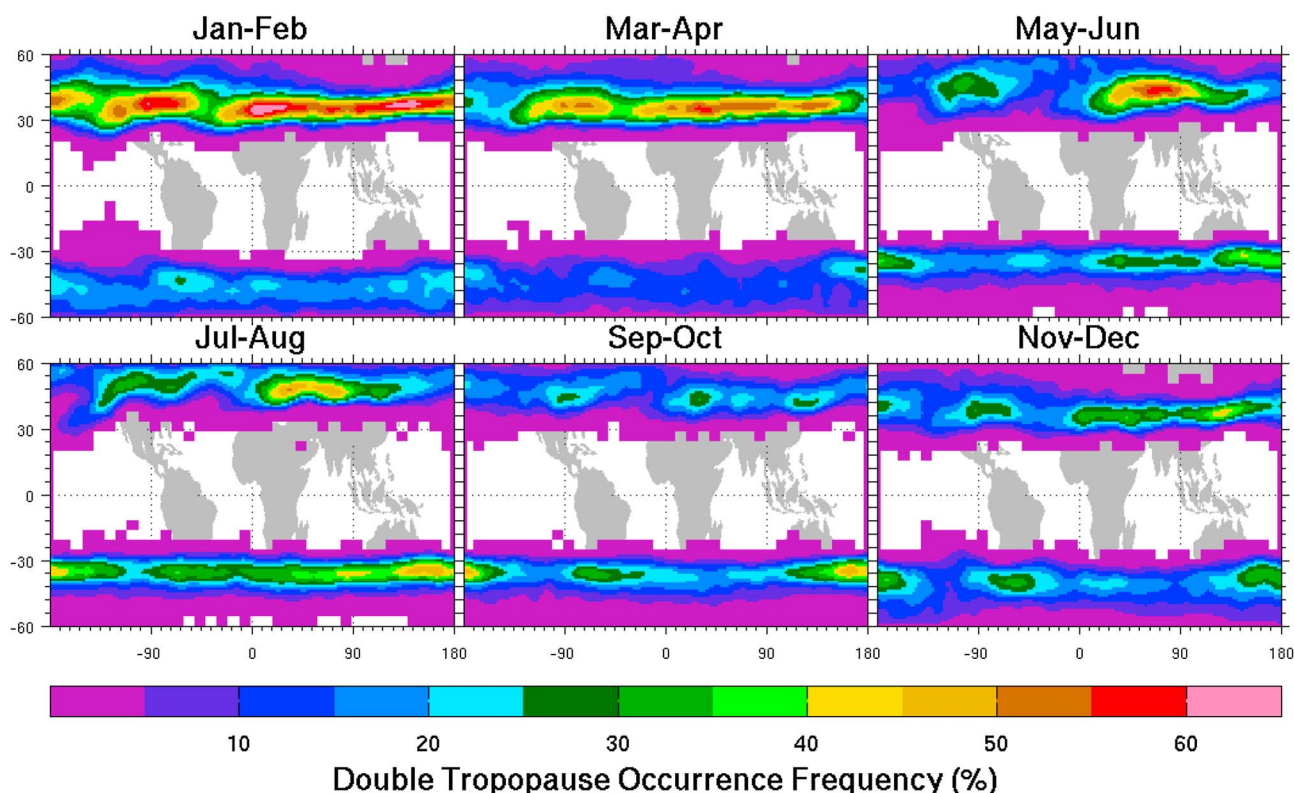
Figure 3. Bimonthly climatologies of occurrence frequencies of double WMO tropopauses from 2005 to 2012 derived from GEOS-5 fields sampled at MLS measurement locations.

Asian and North American monsoons. The longitudinal variations follow those of the upper tropospheric jets (not shown.) NH DT maxima in winter and spring over North America (with a complex pattern of DTs commonly extending to near 60°N) and stretching eastward from north of Africa (with a more zonal pattern confined mainly equatorward of ~45°N) are associated with corresponding maxima in jet frequency distributions, with a pattern of complex, variable jets that split and merge over the eastern Pacific and North America and less variable, more zonal jets over ~0–180°E longitudes [*Manney et al.*, 2014]. SH winter DTs are more zonally symmetric than those of the NH winter, and the highest occurrence frequencies are confined to a narrower-latitude band from ~30 to 45°S. Consistent with previous studies [*Manney et al.*, 2014, and references therein], DT frequencies are larger in the NH than in the SH in corresponding seasons and higher in winter than in summer in a given hemisphere. The STJ shifts poleward in summer, resulting in DTs occurring at higher latitudes than in winter.

2.3. Satellite Sampling of Double- and Single-Tropopause Regions

The representation of DT and ST regions in satellite observations depends critically on their sampling patterns/frequencies. Substantial biases may arise in cases where the sampling is nonuniform with respect to the seasons or the geographic region being examined. Figure 4 shows mean latitudes, occurrence rates, and altitudes of STs and DTs for the ensembles of profiles observed by MLS, HIRDLS, and ACE-FTS that are used in section 3. These sets of profiles are all selected using the extratropical criteria described above. These panels show the general characteristics of seasonal variation in DT locations. As expected, given their similar sampling patterns and daily uniform coverage of midlatitudes, the locations (latitudes and altitudes) of DTs and STs sampled by MLS and HIRDLS are very similar for the most part.

In both hemispheres, the equatorward boundary of the extratropics shifts poleward in summer, in the NH because the STJ shifts poleward, and in the SH because the STJ becomes weak and the polar upper tropospheric jet becomes the main jet across which the large drop in the primary tropopause occurs [e.g., *Manney et al.*, 2014]. Since extratropical DTs are most common close to the STJ, the mean DT is at lower latitude than the mean ST, typically by ~8–10° in winter and spring and ~4–5° in summer; this seasonal difference in the mean DT versus ST latitude is expected because of the contraction of the latitude region considered in summer.
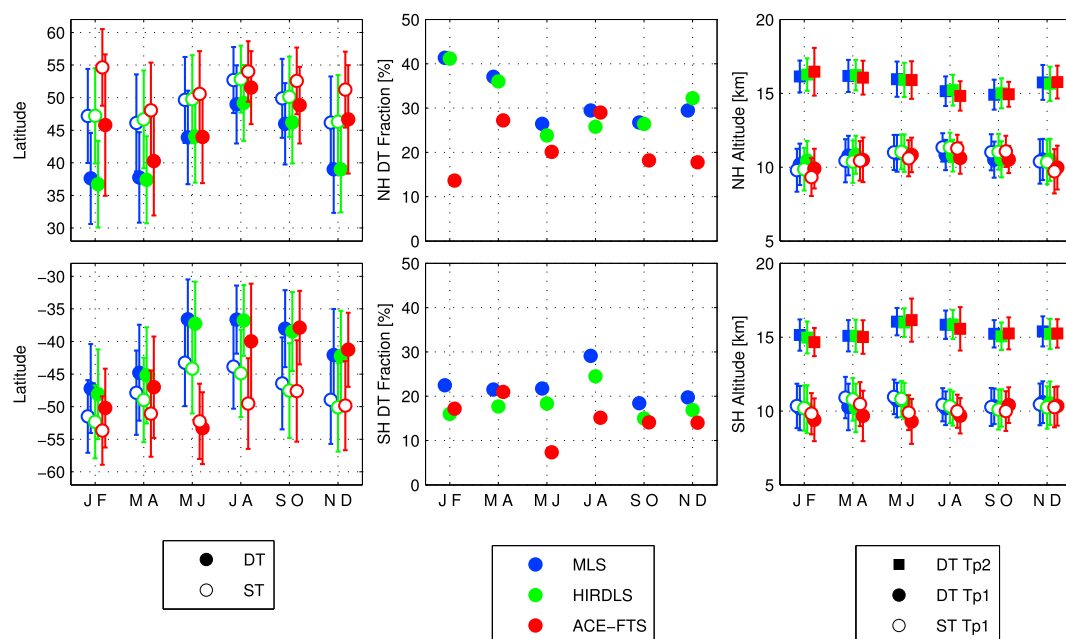
Figure 4. GEOS-5-derived (left column) ST and DT ensemble-mean latitude, (middle column) DT occurrence fraction, and (right column) tropopause altitudes, at measurement locations of MLS (blue), HIRDLS (green), and ACE-FTS (red); NH is above and SH below. Statistics are of extratropical profiles, per the screening described in section 2.2. DT fractions shown in the middle column are the number of extratropical profiles with multiple tropopauses divided by the total number of extratropical profiles. The 1σ variabilities of the binned latitudes and altitudes are shown with error bars. Marker symbols are offset about the bimonthly horizontal tick marks to keep error bars from obscuring one another.

ACE-FTS mean latitudes are generally higher than those of MLS and HIRDLS, particularly in the winter, when the boundary of the tropics retreats equatorward and the ACE-FTS sampling is more focused on high latitudes. A large fraction of DTs observed by MLS and HIRDLS in the winter are just poleward of the STJ, which in winter shifts equatorward to latitudes rarely sampled by ACE-FTS. The winter DTs observed by ACE-FTS are, on average, biased high in latitude, as seen in Figure 4 (left column). The bimonthly averages used here smooth even larger monthly variability; for example, ACE-FTS samples much higher southern latitudes in July than in August.

DT frequencies (Figure 4, middle column) are, except in the NH in ND and JF, lower in HIRDLS than in MLS by ~2–4% in the NH and ~3–5% in the SH. While MLS sampling is quite uniform in latitude through the midlatitudes, HIRDLS midlatitude sampling is biased poleward, particularly in the SH. The seasonal patterns are, however, very similar in MLS and HIRDLS, with a winter maximum in DT occurrence of over 40% in the NH and 25–30% in the SH. MLS and HIRDLS NH DT frequencies drop to 25% in MJ and gradually increase to 30% in ND, while SH DT frequencies drop earlier in the southern late winter/spring to 15–20% in SO, then increase slowly to 20% in MJ. ACE-FTS DT occurrence frequencies are similar to those from MLS and HIRDLS in summer, but they are much lower in September–March in the NH and in May–August in the SH. The ACE-FTS NH JF DT frequency of ~15% is one third that of the other instruments; in MJ in the SH, ACE-FTS samples DTs <10% of the time, about one half the rate of the other instruments. As with the latitude/altitude biases, this difference in DT occurrence frequency arises from the polar winter-focused sampling of ACE-FTS. The biases in sampling of DTs between the instruments, especially the large wintertime biases in ACE-FTS sampling, can also have consequences for diagnosing the trace gas distributions in DT versus ST regions and will be discussed further in the following sections.

3. Single-Tropopause and Double-Tropopause Climatologies
3.1. March NH Profiles
In this section we show NH March DT and ST mean profiles and histograms of trace gases from MLS (2005–2012), HIRDLS (2005–2007), and ACE-FTS (2005–2010) along with several meteorological analysis fields. As shown earlier, extratropical DTs are more common in the NH than in the SH. March is a
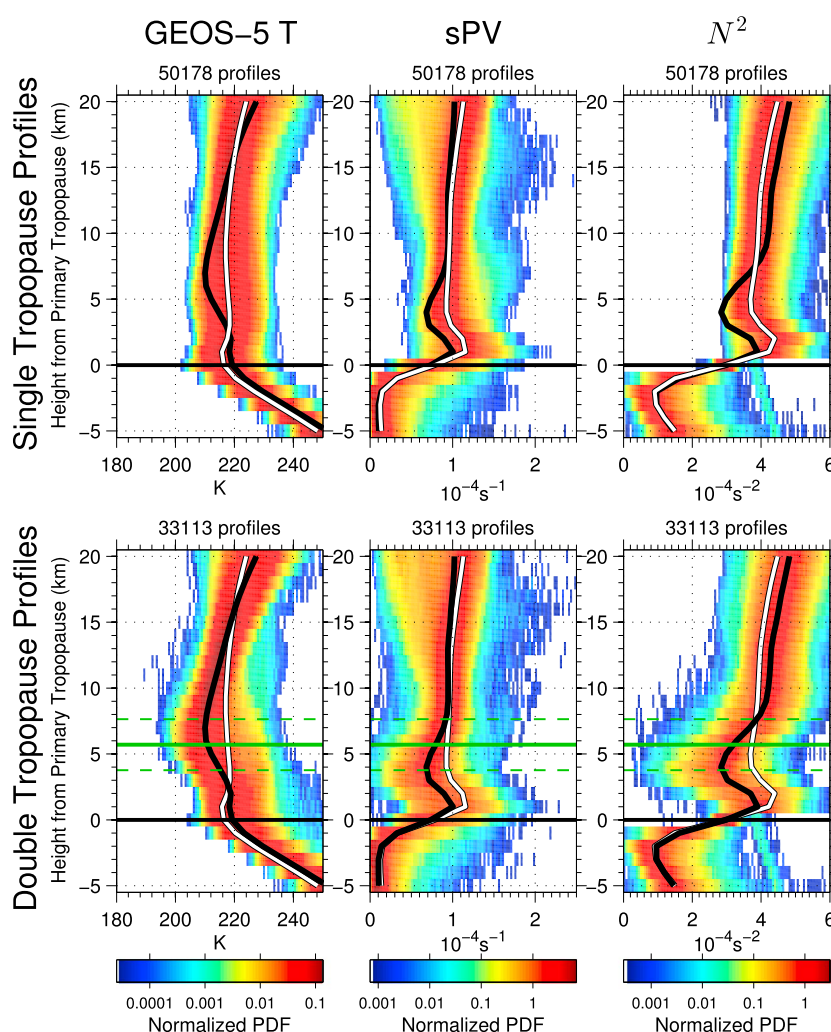
Figure 5. From left to right, temperature, sPV, and N^2 are shown for (top row) ST and (bottom row) DT March NH extratropical MERRA profiles collocated with MLS observations from 2005 to 2012. The vertical axis is the height from Tp1. Colors are occurrence histograms on logarithmic scales, normalized separately at each vertical level. Units are the inverse of those of the horizontal axis so that histograms at each level integrate to unity. The white (black) profile is the single-tropopause (double-tropopause) mean, each shown on both rows to facilitate comparisons. The mean Tp2 height above Tp1 is shown in Figure 5 (bottom row), in green, with 1σ error bars.

representative month, with the third highest monthly rate of NH extratropical DTs (37%), after February (43%) and January (40%).

Figure 5 shows March NH extratropical profile histograms of temperature, sPV, and N^2 from MERRA at MLS measurement locations for ST (top row) and DT (bottom row) cases. Colors are occurrence histograms on a logarithmic scale, providing a representation of the underlying probability distribution functions (PDFs). Here we use height above Tp1 (ZTp1) as the vertical coordinate to preserve, in averaged profiles, the sharpness of vertical structures associated with Tp1 that may be blurred when averaging profiles as functions of height from the Earth surface (Zsfc) [*Pan et al.*, 2004, 2006; *Hegglin et al.*, 2009, and references therein].

Profiles are extratropical, as described above, and ST and DT Tp1s have similar mean heights and 1σ variability: 10.2 ± 1.5 km for ST cases and 10.6 ± 1.4 km for DT cases. While Tp1 of the composited DT profiles are aligned with one another, by definition, when using ZTp1 as the vertical coordinate, the composite Tp2 is somewhat blurred by variability in the intertropopause distance, so the mean Tp2 height does not correspond precisely to the height at which the temperature lapse rate of the mean profile drops below 2 K/km.

The mean Tp1 for the ST cases is colder and sharper than that for the DT cases. The mean Tp2 for the DT cases is colder than Tp1 by ~8 K, more closely resembling a tropical than an extratropical tropopause both in height and in temperature.

The sharp increase in sPV with increasing height across Tp1 arises from the rapid increase in N^2 at the primary tropopause. In the first 10 km above Tp1, fewer than 0.05% of ST sPV values are less than 0.5×10^{-4} s^{-1}, and fewer than 2% of sPV values are less than 0.7×10^{-4} s^{-1}, consistent with the transition between red and yellow in the PDF of Figure 5 (top middle) corresponding to ~2σ below the mean of a Gaussian distribution. In the DT case, the mean value 4 km above Tp1 drops to 0.6×10^{-4} s^{-1} with more than 2% of values below 0.2×10^{-4} s^{-1} and minimum values down to 0 s^{-1}, characteristic of air from several kilometers below the tropopause and/or well into the tropics. These low values of sPV from ~2 to 7 km above Tp1 are consistent with the intrusion of low-latitude and/or tropospheric air into the intertropopause region, as has been described previously in case studies [e.g., *Pan et al.*, 2009; *Vogel et al.*, 2011; *Ungermann et al.*, 2013]. The peak in N^2 just above Tp1 that defines the TIL is evident in both DT and ST profiles; it is also reflected in sPV due to its dependence on N^2. While peak TIL N^2 values are lower in DT than in ST cases, the intrusion low-N^2, low-sPV sPV air just above the TIL makes the "inversion" defined by the gradient of N^2 even stronger. The case studies of *Pan et al.* [2009] showed similar N^2 profiles through the tropopauses.

Figure 6 shows extratropical mixing ratio climatologies of MLS v3 trace gases from March 2005–2012 for ST and DT regimes. O_3, HNO_3, and HCl are stratospheric tracers, with their primary sources and highest mixing ratios in the middle atmosphere. Their mixing ratios increase with height above Tp1 in the ST case (top row and white mean lines). DT profiles of these species have low values characteristic of air of tropospheric and/or tropical origin at and just below Tp2. The differences between their mean ST and DT profiles have maxima of ~0.5 ppmv, ~2 ppbv, and ~1.5 ppbv, respectively, near the height of Tp2.

Use of ZTp1 rather than Zsfc as the vertical coordinate better resolves compositional features associated with tropopause structure but may contribute to spurious DT-ST differences higher in the stratosphere. Vertical shifts resulting from slightly different mean Tp1 heights of the DT and ST ensembles can result in apparent DT-ST differences (with respect to ZTp1) that are merely differences of shifted, common (with respect to height from the surface) vertical structures, such as the peak in stratospheric HNO_3 at ~25 km altitude. Differences in latitudinal sampling of the DT and ST ensembles can also result in significant DT-ST differences for species with large latitudinal gradients and are likely responsible for the higher ST HNO_3 values in the stratosphere. In section 3.2, care will be taken to minimize such latitudinal sampling artifacts, and it will be shown that the remaining DT-ST differences are very small fractions of the average mixing ratios at altitudes more than 10 km above Tp2.

CO is a tropospheric tracer with mixing ratios that generally decrease with height in the UTLS and drop more sharply at the extratropical tropopause. UT CO climatological values are higher in the NH, where most of the CO sources are located, and they have a strong, poleward increasing, meridional gradient in the NH winter, when there are more anthropogenic sources and there is a smaller photochemical sink [e.g., *Hegglin et al.*, 2009]. UT CO has considerable geographic variability, since locally high values can result from episodic convective injection from a variably polluted boundary layer [e.g., *Jiang et al.*, 2007; *Duncan et al.*, 2007], but its average values are still significantly higher in the TTL than in the lower stratosphere, so it is expected to behave as a tropospheric tracer, with elevated mixing ratios marking injection of TTL air into the intertropopause layer. The MLS March ST and DT mean CO climatologies are very similar to one another, with only very slightly higher values in the DT case in a ~3 km layer just above Tp1. Comparisons of zonal mean CO from MLS, ACE-FTS, and the Envisat Michelson Interferometer for Passive Atmospheric Sounding (M. I. Hegglin and S. Tegtmeier (Eds.), SPARC Data Initiative: Assessment of stratospheric trace gas and aerosol climatologies from satellite limb sounders, SPARC Report No. 7, manuscript in preparation, 2015) show latitudinal gradients in MLS v3 CO that are inconsistent with those expected and seen in data from the other instruments, suggesting possible deficiencies in the MLS v3 CO product. This inconsistency is discussed further in section 3.2.5 in the context of seasonal climatologies.

The troposphere is much wetter than the stratosphere, but transport of TTL air into the LMS does not typically result in wet anomalies. Extremely low temperatures in the TTL "freeze dry" air parcels, so parcels entering the LMS from the TTL in DT regions are dry relative to ST parcels that have been moistened by methane oxidation during their longer stratospheric residence [e.g., *Krebsbach et al.*, 2006]. This can be seen in Figure 6, where the DT mean profile is ~0.6 ppmv drier than the ST mean profile within 2 km of Tp2. The
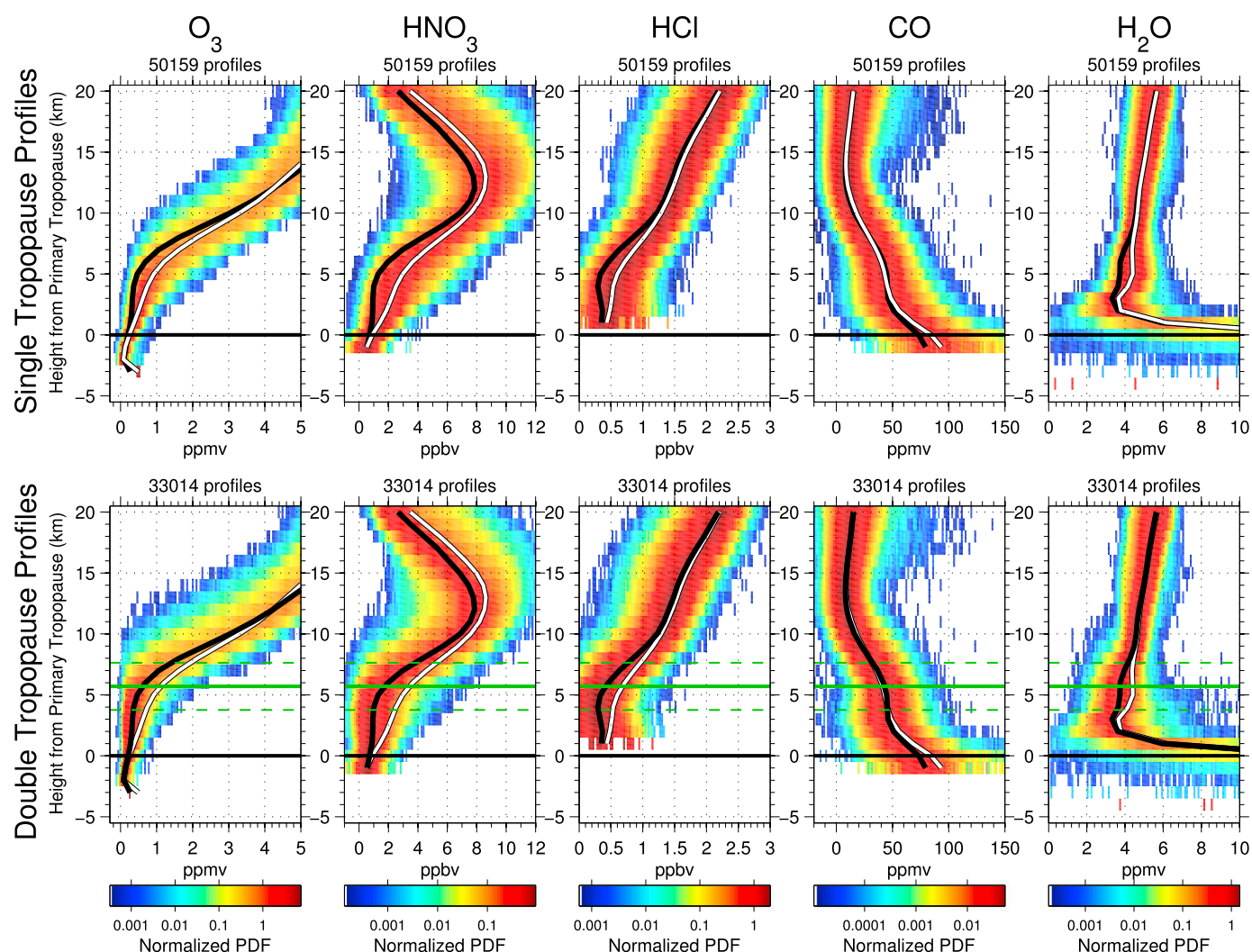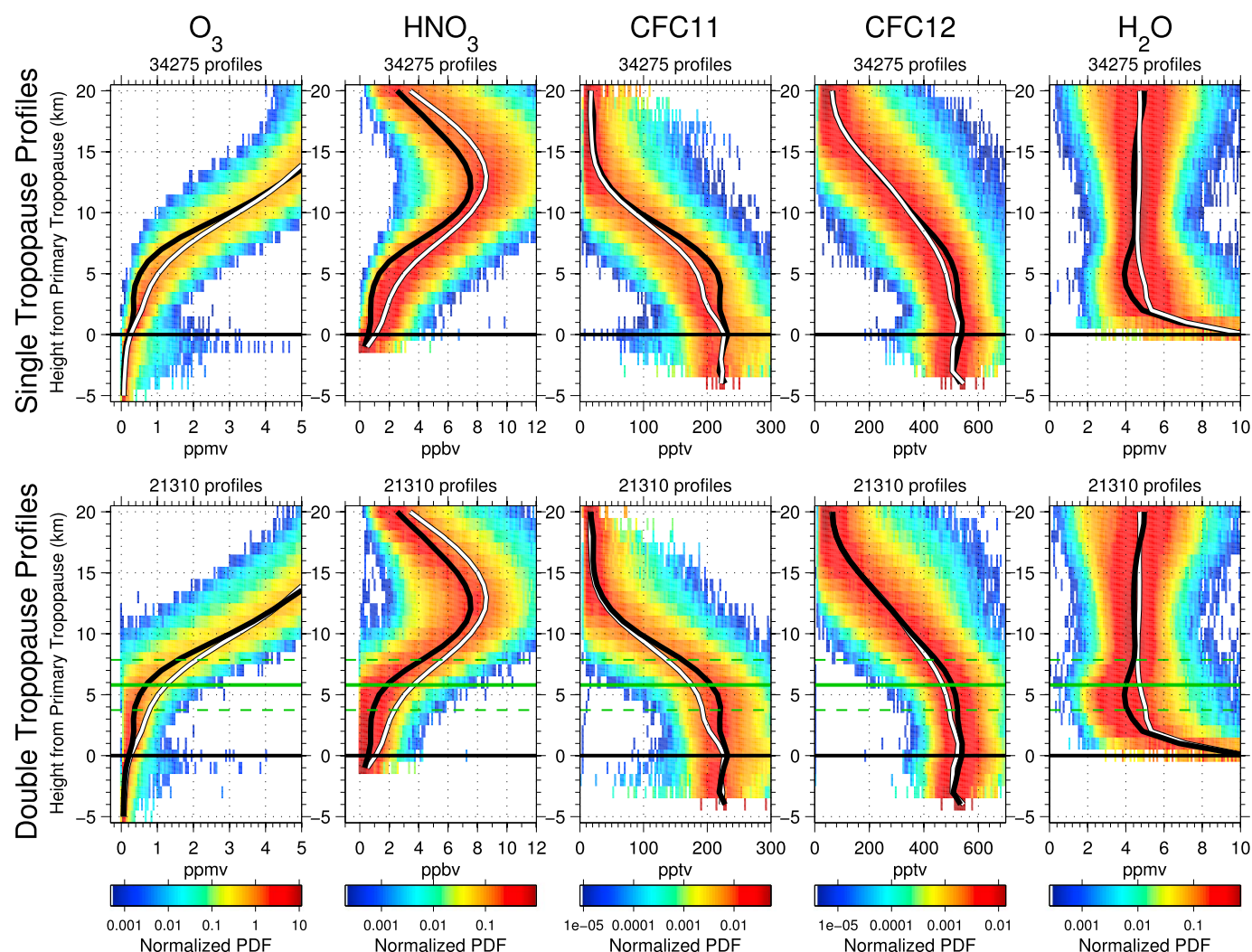
Figure 6. MLS March 2005–2012 climatologies of NH extratropical trace gases for (top row) single-tropopause and (bottom row) double-tropopause profiles; plot format is otherwise as used in Figure 5.

2.5–3 km vertical resolution of the MLS H$_2$O measurements can result in an appreciable contribution from wet layers just below the tropopause into retrieved values in the first few kilometers above the primary tropopause, complicating interpretation of the measurements in this region. With these caveats, the behavior of MLS H$_2$O appears to be generally consistent with the transport of significant amounts of air from the TTL into the LMS layer between the extratropical DT tropopauses. Below, we show similar analyses using the HIRDLS and ACE-FTS data to explore the consistency of the data sets and assess possible sampling issues.

Figure 7 shows March climatological (2005–2007) extratropical ST and DT profiles of HIRDLS O$_3$, HNO$_3$, CFC-11, CFC-12, and H$_2$O. HIRDLS has better vertical resolution (~1 km) than MLS, and for some species, it is sensitive slightly farther down into the troposphere (to 7–9 km from the surface when not obscured by clouds), but the obstructed HIRDLS aperture complicates calibration, and the unrelated failure of the chopper limited observations to just over 3 years [*Gille and Gray*, 2013]. The HIRDLS O$_3$ and HNO$_3$ ST and DT ensembles are very similar to those shown for MLS in Figure 6, both in mean values and in their PDFs. Outliers seen near Tp1 in both ST and DT ensembles of O$_3$ (as well as in CFC-11 and CFC-12) are not seen in the MLS O$_3$ and are likely spurious. The most significant difference between the MLS and HIRDLS plots is an even larger persistent HIRDLS DT-ST HNO$_3$ deficit through the middle stratosphere. HIRDLS extratropical latitudinal sampling is less uniform than that of MLS and may exacerbate the latitudinal sampling issue discussed above in connection with Figure 6.

Figure 7. HIRDLS March 2005–2007 climatologies of NH extratropical trace gases for (top row) single-tropopause and (bottom row) double-tropopause profiles; plot format is otherwise as used in Figure 5.

Consistent with the patterns seen in the MLS profiles, HIRDLS DT profiles of the stratospheric tracers, O_3 and HNO_3 (black lines), have significantly lower mean values between the tropopauses and just above Tp2 than the ST profiles (white lines) at the same heights above the primary tropopause. DT mean values are nearly constant from just above Tp1 to ~1–2 km below Tp2, at values slightly higher than those in the troposphere. The close agreement between HIRDLS and MLS O_3 and HNO_3 indicates that the coarser MLS vertical resolution does not prevent it from capturing the essential features of the UTLS structure or significantly bias the magnitude of the differences between DT and ST profiles. Small quantitative differences in O_3 and HNO_3 climatologies from MLS and HIRDLS are to be expected given that the HIRDLS record only covers 3 years.

The tropospheric tracers CFC-11 and CFC-12 have significantly higher mixing ratios between the tropopauses for the DT cases than at the same heights above the primary tropopause in the ST cases. CFC-11 has a shorter mean stratospheric lifetime than CFC-12 (52 years and 102 years, respectively [*Ko et al.*, 2013]), leading to a steeper vertical gradient as a fraction of tropospheric abundance and a larger ratio of ST to DT values 2–8 km above Tp1. In the ~2 km layer just above Tp1, ST and DT mean profiles are quite similar, consistent with the supposition that tropospheric air primarily enters the intertropopause region above, but not through the TIL.

The HIRDLS H_2O product is newly available in v7 and thus has not been extensively validated, but initial comparisons with Cryogenic Frost-point Hygrometer sondes [*Vömel et al.*, 2007], ACE-FTS, and MLS are

promising [*Gille and Gray*, 2013]. The mean value for HIRDLS H_2O in ST profiles is nearly constant at ~5 ppmv at heights from 2 to 20 km above Tp1, compared to a significantly lower value (~3.5 ppmv) from MLS 2–4 km above Tp1 that increases to ~5 ppmv about 8 km above Tp1 then gradually to ~6 km at 20 km above Tp1. This gradual stratospheric increase with height in MLS values is expected from the increasing contribution of methane oxidation [*Jones et al.*, 1986]. Near 100 hPa (about the height of Tp2), MLS H_2O has been shown to agree well with mean H_2O derived from a multinational set of satellite instruments for the SPARC Data Initiative [*Hegglin et al.*, 2013], suggesting a high bias in the HIRDLS data at this level. Near 200 hPa, *Hegglin et al.* [2013] reported a low bias in MLS H_2O compared to the multi-instrument mean, which may be reflected in the deeper minimum in MLS profiles 2–3 km above Tp1 that is seen in Figure 6 but not present in the HIRDLS profiles. The scatter of the HIRDLS data about its mean is considerably larger than that for MLS in the vicinity of the tropopause(s) (the 1σ scatter 2–5 km above the primary tropopause is ~0.6 ppmv for MLS and ~1.2 ppmv for HIRDLS), even though the estimated precision of each instrument's data is similar (~0.3 ppmv). This may reflect additional atmospheric variability captured by HIRDLS because of its finer vertical resolution but could also arise from the calibration challenges of the HIRDLS measurement system. Despite these differences arising from data quality and resolution issues, MLS and HIRDLS are consistent in having DT profiles systematically drier than ST profiles by up to ~0.5 ppmv just below and through the height of Tp2.

ACE-FTS is a solar occultation instrument, with the sensitivity advantages that accrue from viewing the atmosphere in absorption against a very bright source; it also achieves somewhat better resolution in the UTLS than its nominal 3–4 km resolution at higher altitudes [*Hegglin et al.*, 2008]. However, the sparse sampling (up to 15 sunrises and sunsets per day) and sampling pattern optimized for NH high-latitude observations severely limit the coverage of low and middle latitudes and may bias some of the results shown below, as was discussed in sections 2.1 and 2.3.

Figure 8 shows March ST and DT ACE-FTS profiles of O_3, HNO_3, methane (CH_4), CO, and H_2O. There are only 179 NH extratropical ACE-FTS March profiles in the period 2004–2010, while 83,000 profiles are used to produce Figure 6 for MLS and 55,000 profiles are used to produce Figure 7 for HIRDLS. (The number of profiles used to produce each panel of Figures 6–8 is included in the panel title.) Despite the extreme sparsity of the ACE-FTS sampling (particularly an issue when, as we are doing, high latitudes are excluded), the ACE-FTS mean extratropical profiles are remarkably consistent with those from MLS and HIRDLS. The ACE-FTS O_3 and HNO_3 ensembles have very similar mean values to those seen for MLS and HIRDLS. ACE-FTS HCl (not shown) also shows distributions very consistent with those from MLS.

ACE-FTS CH_4 begins to decrease with height at Tp1 in the ST cases and at Tp2 in the DT cases, in a manner similar to that seen in other tracers with tropospheric sources (cf. HIRDLS CFC-11 and CFC-12 in Figure 7). ACE-FTS ST CO is ~10 ppbv higher in the DT case than in the ST case at heights 2–8 km above Tp1, consistent with what is expected if parcels with elevated CO are entering the intertropopause layer of the DT profiles. Both DT and ST profiles from MLS have higher mixing ratios than those from ACE-FTS 2–10 km above Tp1, with ACE-FTS lower than MLS in the ST mean by 20–30 ppbv at heights ~2–6 km above Tp1. MLS DT CO has similar curvature to ACE-FTS DT CO, with higher values near Tp2 and lower values just above Tp1 than in the ST profile, but the overall MLS DT-ST differences through the tropopause region are less positive than those of ACE-FTS by ~10 ppbv.

ACE-FTS H_2O has minima in both the mean DT and ST profiles ~5 km above Tp1 (2.5 ppmv for DT and 3.5 ppmv for ST mean profiles) that are slightly drier than the means from MLS and HIRDLS at the same level and are closer to the multi-instrument mean compiled for the SPARC Data Initiative [*Hegglin et al.*, 2013]. Like HIRDLS H_2O, ACE-FTS H_2O lacks the low notch seen in MLS H_2O 2–3 km above Tp1 that is believed to result from the previously reported low bias in MLS at 215 hPa [*Hegglin et al.*, 2013]. However, despite biases in mean values, the negative difference between DT and ST means in ACE-FTS H_2O profiles in the region within 2 km of Tp2 is consistent with those seen in MLS and HIRDLS.

To summarize, the three instruments provide a consistent picture of the influence of tropopause multiplicity on the ensemble of trace gas distributions examined for the example shown, March in the NH. Results are consistent with the presence of low-latitude/tropospheric air in the upper portion of the layer between double tropopauses. The next section will expand this analysis to show the seasonal and interhemispheric variability in trace gases in DT versus ST regions.
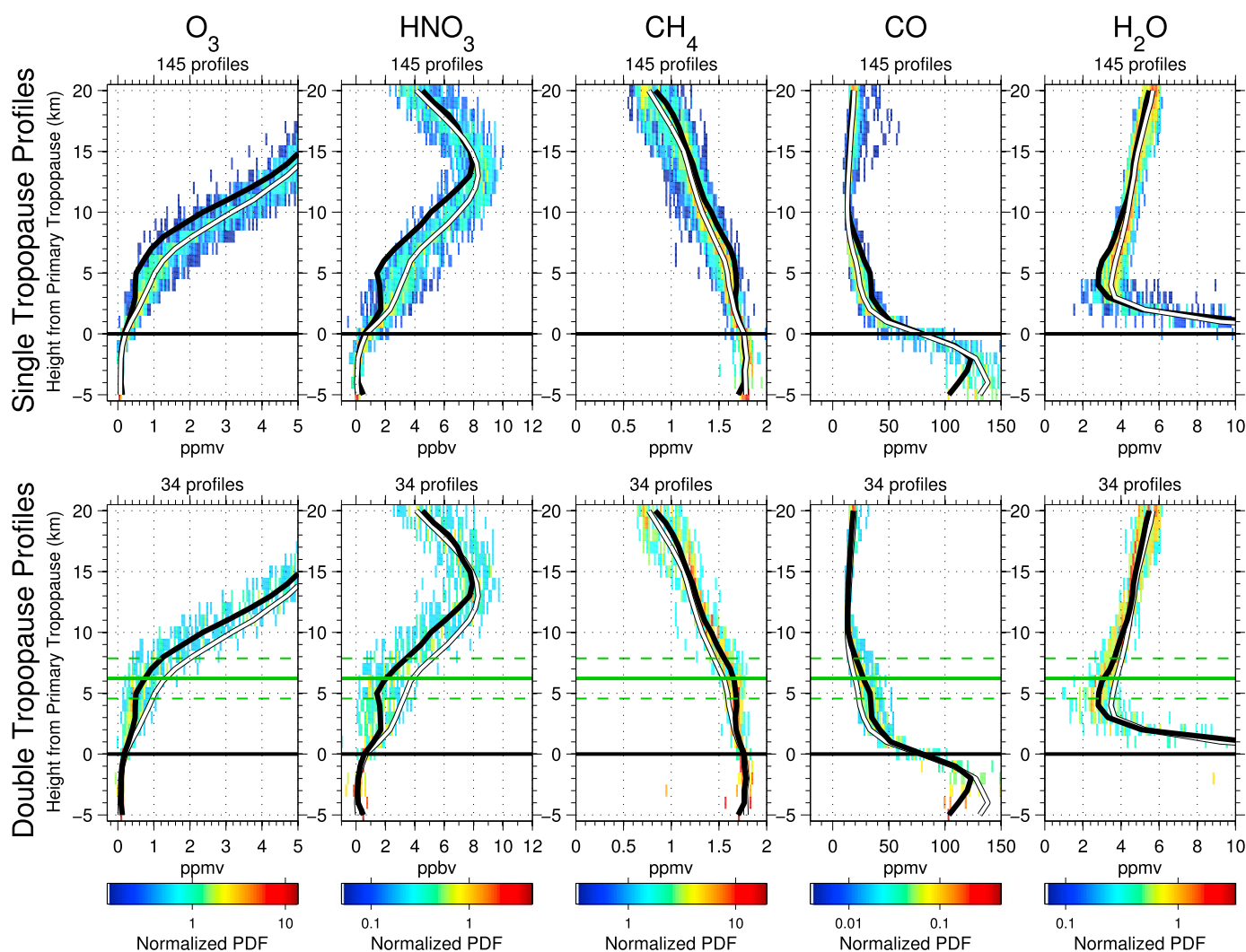
Figure 8. ACE-FTS March 2005–2010 climatologies of NH extratropical trace gases for (top row) single-tropopause and (bottom row) double-tropopause profiles; plot format is otherwise as used in Figure 5.

3.2. Seasonal and Interhemispheric Variations

Figures 9–14 show the seasonal variability of extratropical mean climatological profiles and DT-ST profile differences of trace gases and meteorological fields of interest. The "mean profiles" are bimonthly averages of all extratropical DT and ST profiles in a given hemisphere; they are used as the denominator in calculation of fractional difference profiles, DT-ST%. Care has been taken to minimize the degree to which DT-ST differences reflect latitudinal gradients found in some tracers, since DT cases are, on average, sampled at lower latitudes than ST cases, as is shown in Figure 4. The differences shown are formed by first constructing zonal mean differences within narrow (5°) latitude bins and then averaging these differences, weighted by the prevalence of DTs within the bins. Bins with few DT profiles will thus be weighted lightly. To avoid the possibility of using 55° averages from bins in which there are very few ST profiles (where effects of precision and outliers could be problematic), bins are rejected if they contain fewer than 25 ST profiles for MLS or HIRDLS or fewer than five profiles for ACE-FTS. The lower threshold for ACE-FTS is necessitated by the sparseness of its measurements and is somewhat justified by the excellent individual measurement precision of its solar occultation technique.

3.2.1. Scaled Potential Vorticity

The GEOS-5 sPV climatology, shown for the two hemispheres in Figure 9 (left column), has the expected sharp transition between low tropospheric values and higher stratospheric values at Tp1. The peak at the TIL is largest in summer, when the extratropical TIL is strongest [e.g., *Grise et al.*, 2010]). DT-ST sPV differences
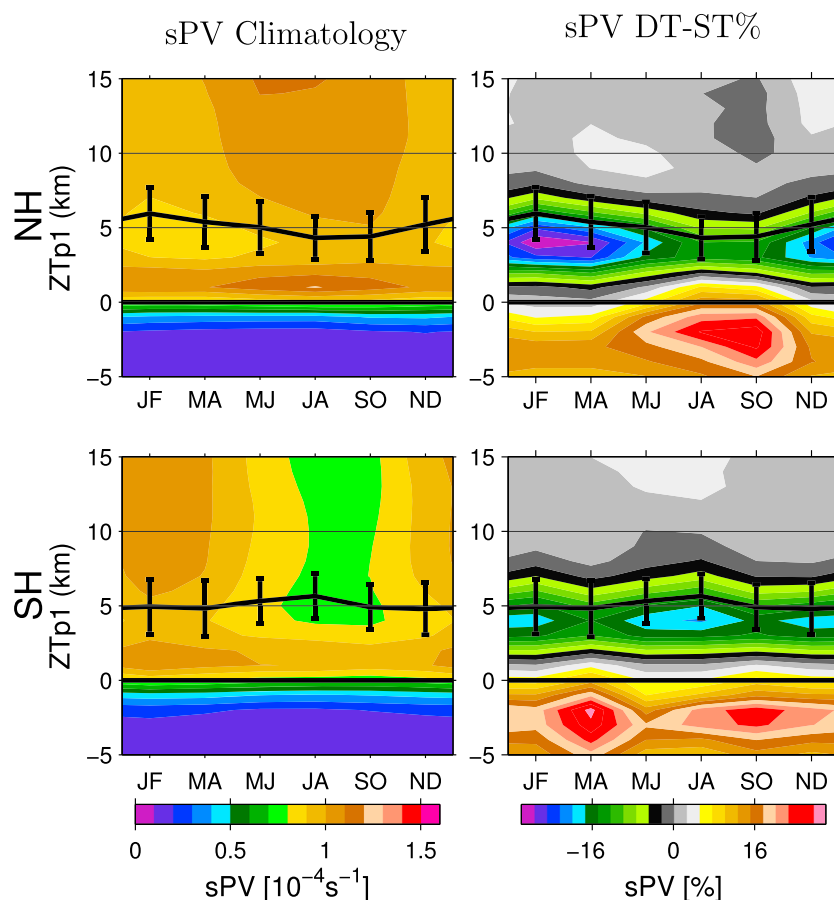
Figure 9. (left column) Climatological mean sPV and (right column) DT-ST% sPV from GEOS-5, interpolated to the locations of MLS extratropical observations, for the (top row) NH and (bottom row) SH. Profiles are plotted as a function of height from Tp1. Tp2 height (relative to Tp1) is shown by a black line with error bars indicating ensemble variability. This Tp2 line is included on the climatological mean plots as a guide to the eye.

sampled at MLS measurement locations (Figure 9, right column) show that in all seasons, sPV is lower in the 3 km just below Tp2 in DT profiles than it is at the same level in the ST profiles, consistent with the intrusion of low-latitude and/or tropospheric air into this layer. The NH seasonal cycle of this intrusion signature has a winter peak magnitude greater than $0.2 \times 10^{-4} \mathrm{s}^{-1}$, which is more than 30% of the mean value at this level. These clear, seasonally varying dynamical features in sPV from the GEOS-5 analysis will be seen reflected in the satellite-based trace gas DT-ST seasonal patterns, below.

3.2.2. Ozone

Figure 10 (left column) shows MLS extratropical mean climatology with respect to ZTp1. The seasonal cycle in O_3 is largely governed by the seasonal cycle in the Brewer-Dobson circulation (BDC), which is stronger into the winter hemisphere than into the summer hemisphere and stronger into the NH than the SH [e.g., *Shepherd*, 2002]. This seasonal cycle brings higher values of O_3 down to lower levels of the winter hemisphere. A stronger BDC also pushes the tropical tropopause (and its extension as the extratropical Tp2) upward and pushes the high-latitude Tp1 downward, resulting in the observed seasonal cycle in the height of Tp2 relative to Tp1.

DT-ST% O_3 differences with respect to ZTp1 are shown for MLS, HIRDLS, and ACE-FTS in the second to fourth columns of Figure 10. These panels demonstrate very consistent results from the MLS and HIRDLS measurements, even 10–15 km above Tp1, where O_3 has strong vertical gradients. These DT-ST% signals are robust, despite the different measurement periods. Indeed, MLS DT-ST% plots from data limited to the HIRDLS 3 year time period (not shown) are very similar to those produced from the first 9 years of MLS data for all MLS species used in this work. ACE-FTS O_3 results are broadly consistent with those from MLS and HIRDLS, with differences likely arising from the sparse ACE-FTS sampling in the region of interest. ACE-FTS sampling is
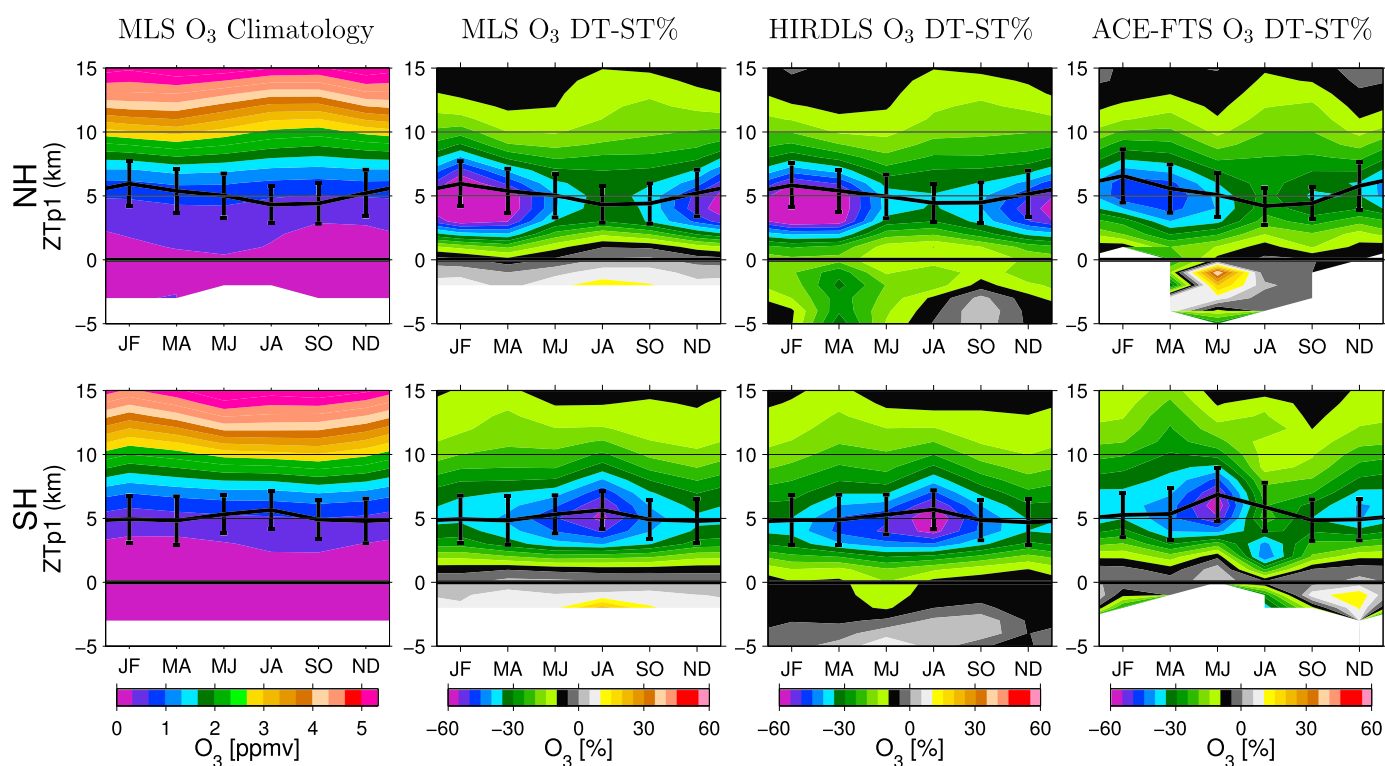
Figure 10. (first column) MLS extratropical, climatological mean O$_3$ and (second column) MLS, (third column) HIRDLS, and (fourth column) ACE-FTS O$_3$ extratropical mean DT-ST profiles as a fraction of each instrument's mean profile for the (top row) NH and (bottom row) SH. All profiles are plotted as a function of height from Tp1. Tp2 height (relative to Tp1) is shown in black with error bars indicating ensemble variability. A Tp2 line is included on the climatological mean plots that shows Tp2 of the DT profiles that, along with ST profiles, contribute to the mean.

biased to high latitudes, particularly in SH fall/winter, where the largest discrepancies occur. Here the few DTs sampled by ACE-FTS correspond to the extreme highest latitude DTs seen by MLS and HIRDLS; these DTs would be less influenced by posited in mixing from the TTL leading to the much smaller DT-ST% differences than seen with MLS of HIRDLS near Tp2 in SH May through August.

The pattern of negative DT-ST% in O$_3$ suggests a large influx of low-latitude and/or tropospheric air into the region between the two tropopauses. The largest effects are seen ~0–2 km below Tp2 (~3–5 km above Tp1) in winter. MLS and HIRDLS both show negative peak magnitudes of DT-ST% at and slightly below Tp2 in winter/spring of over 50% in the NH and near 50% in the SH. Given that the fraction of profiles with double tropopauses in NH winter is ~40% (as shown in Figure 4), a difference of over 50% in mean DT-ST profiles implies that the presence of DTs reduces the climatological O$_3$ values by as much as ~20% compared to "unperturbed" lowermost stratospheric values. In SH winter, the presence of DTs in ~30% of the profiles leads to an ozone reduction of as much as 10%.

Figure 11 (top) shows a map of the distribution of DT-ST O$_3$ in NH winter, with extensive areas in the NH with DT-ST difference magnitudes greater than 250 ppbv, peaking over continental landmasses. Similar patterns exist in November/December and March/April (not shown). These maximal DT-ST regions are poleward of maxima in DT occurrence, where there is large variability in the jets and in DT occurrence [*Manney et al.*, 2014]. The regions over western North America and western Europe are favored locations for strong upper tropospheric blocking ridges [e.g., *Martius et al.*, 2009; *Woollings et al.*, 2010a, 2010b] and associated Rossby wave breaking. The Rossby wave breaking can, in turn, lead to extensive transport of tropical/subtropical air into the extratropics [e.g., *Nakamura*, 2007; *Shuckburgh et al.*, 2009; *Homeyer and Bowman*, 2013]. NH DT-ST O$_3$ differences in July through October (not shown) are also slightly larger over North America than in other regions, while SH differences are more zonally symmetric in all seasons (shown only for January–February). We note that while, as discussed by *Manney et al.* [2014], the incidence of DT profiles is enhanced along the poleward edge of the Asian summer monsoon, the magnitude of the DT-ST differences in this region does not stand out in corresponding July–August maps of O$_3$ or H$_2$O (not shown). Because the westerly
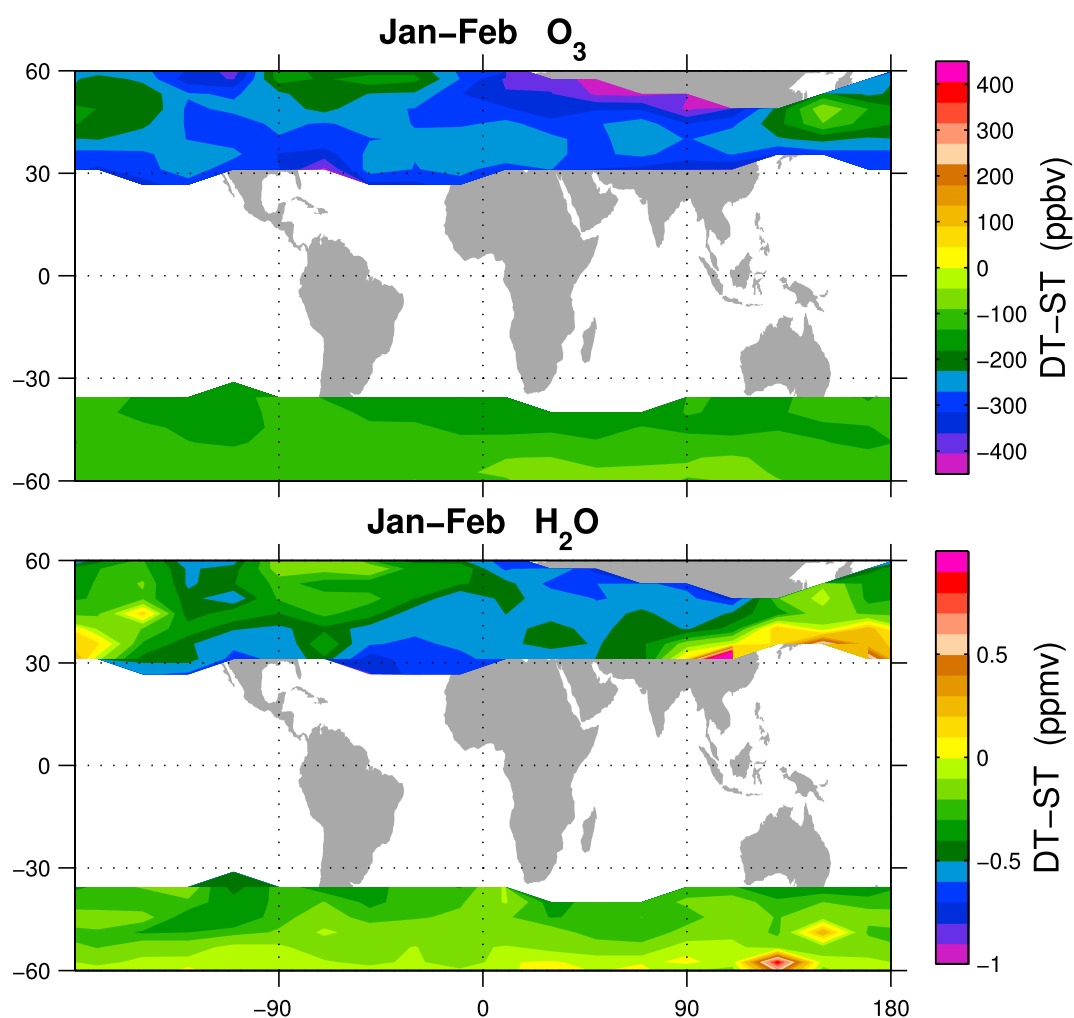
Figure 11. Bimonthly January–February climatologies (2005–2012) of DT-ST for (top) MLS O_3 and (bottom) H_2O at 4 km above Tp1.

subtropical jet shifts poleward, north of the monsoon anticyclone [e.g., *Schiemann et al.*, 2009; *Manney et al.*, 2014], profiles actually within the monsoon are generally considered tropical and thus are not included in this analysis.

### 3.2.3. Nitric Acid and Hydrochloric Acid

MLS mean and DT-ST% climatologies of two other stratospheric tracers, HNO_3 and HCl, are shown in Figure 12. HIRDLS HNO_3 plots are very similar to those from MLS and are not shown. ACE-FTS results for both HNO_3 and HCl (not shown) are also consistent with those for MLS, within the limitations of the ACE-FTS sampling (as discussed above for O_3). The climatologies of HNO_3 and HCl (first and third columns) and O_3 (Figure 10, left column) have different seasonal cycles in the stratosphere, with impacts of summer photolysis in the case of HNO_3 and spring in mixing of polar-processed air in the case of HCl contributing to their differences, but the DT-ST% seasonal patterns of HNO_3 and HCl are quite similar to those of O_3, with negative peak magnitudes of DT-ST% at and slightly below Tp2 in the NH (SH) winter/spring of over (near) 50% in HNO_3 and near 50 (30)% in HCl. The consistency of these DT-ST% seasonal patterns supports the evidence seen in the O_3 distributions that the evolution of the trace gases in midlatitude DT regions is primarily controlled by seasonal patterns in the dynamics that determines the influx of low-latitude and/or tropospheric air into the region between the two tropopauses and less on the details specific to the individual trace gases. As was seen in O_3, the differences in mean DT-ST profiles imply that the presence of DTs reduces the climatological HNO_3 and HCl values by up to ~20% (~10%) in the NH (SH) compared to unperturbed values.
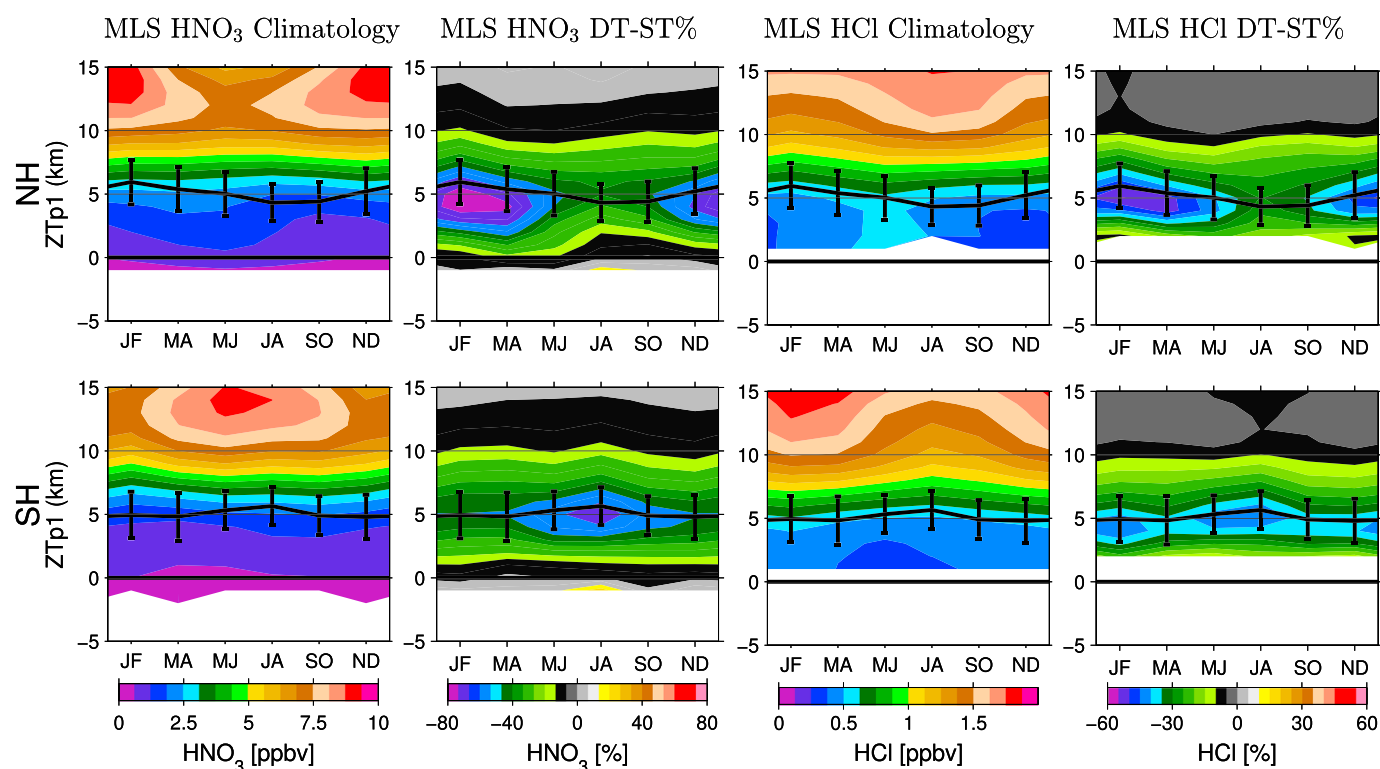
Figure 12. MLS extratropical climatological mean profile and DT-ST as a fraction of mean profile for (first and second columns) HNO_3 and (third and fourth columns) HCl for the (top row) NH and (bottom row) SH. Profiles are plotted as functions of height from Tp1 with Tp2 plotted as in Figure 9.
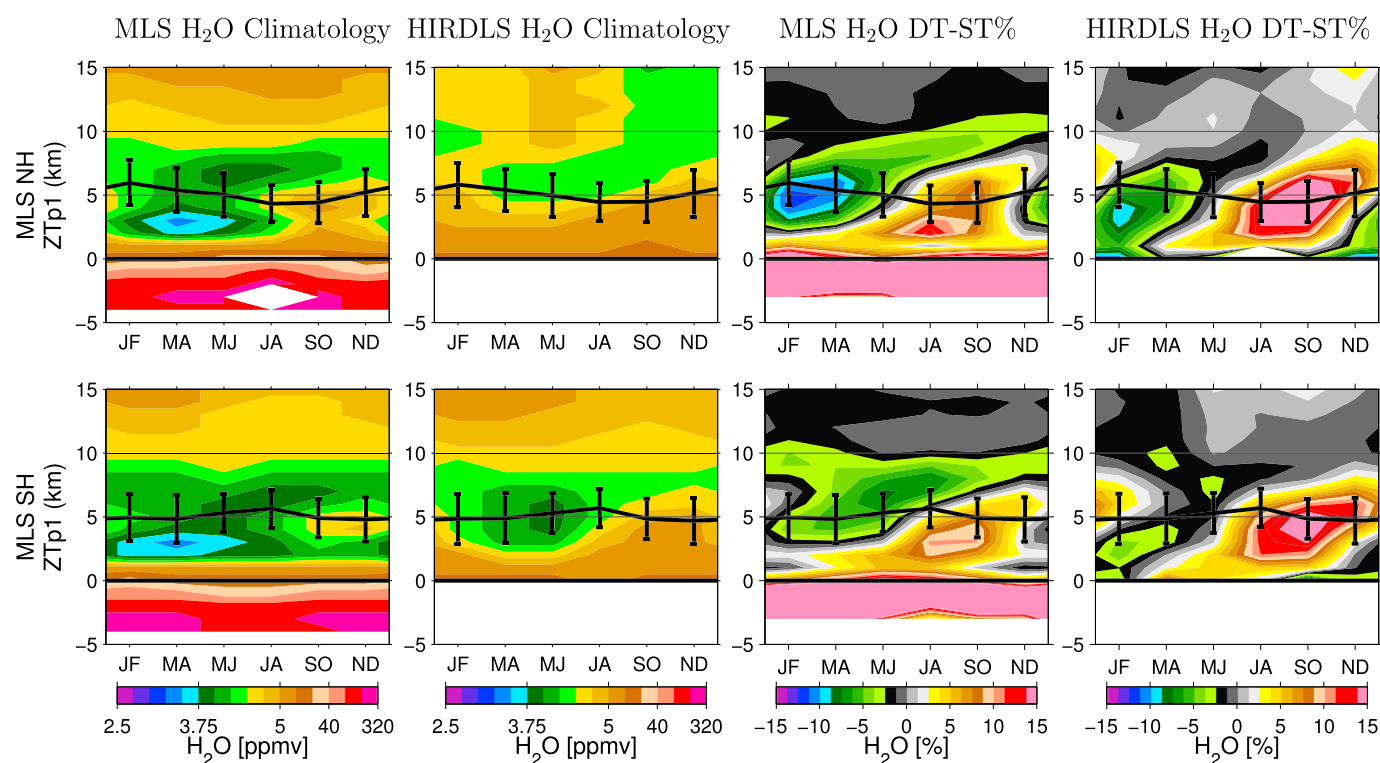
Figure 13. Extratropical bimonthly mean H_2O climatologies from MLS and HIRDLS and MLS and HIRDLS DT-ST differences as fractions of climatology. (top row) NH and (bottom) SH. All profiles are functions of height from Tp1. Color scale for the mean climatologies is linear from 2.5 to 5 ppmv and then is logarithmic, with each successive color a factor of 2 increase, to allow details to be seen at low values while covering the extremely large H_2O dynamic range.
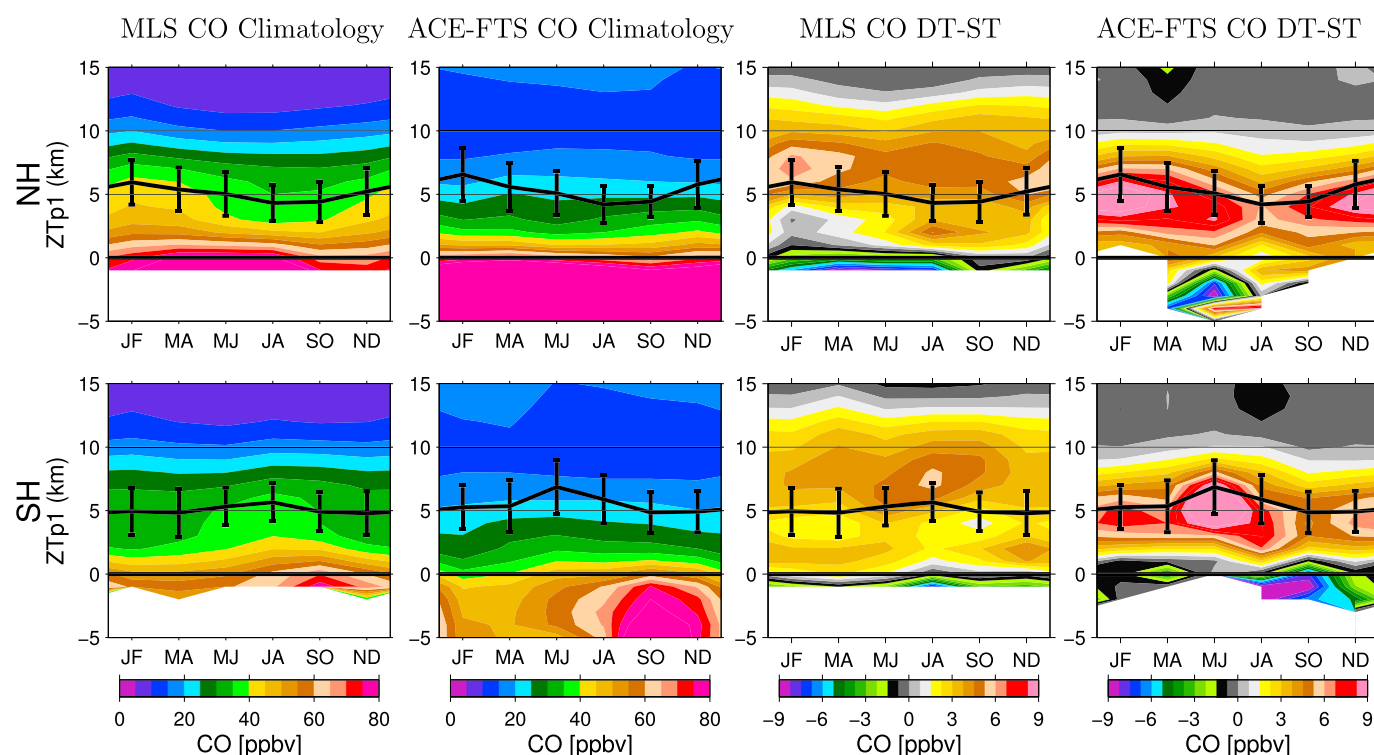
Figure 14. MLS and ACE-FTS CO extratropical bimonthly mean (first and second columns) climatologies as a function of height from Tp1 for all ST and DT profiles and (third and fourth columns) MLS and ACE-FTS DT-ST CO profiles for the (top row) NH and (bottom row) SH. The mean Tp2 height above Tp1 is shown in black, with error bars indicating variability, as in Figure 9.

3.2.4. Water Vapor

Figure 13 shows MLS and HIRDLS H_2O climatological mean profiles (first and second columns, respectively) and DT-ST% (third and fourth columns, respectively). Note that the color scale of the mean climatologies is logarithmic above 5 ppmv to cover the large dynamic range of values. ACE-FTS also has an H_2O product, but its temporal and latitudinal sampling is not sufficient to produce significant results in all seasons, and it is not shown. Unlike the other species that have been examined, for which climatological variability is roughly 6 months out phase between NH and SH, the seasonal cycle of H_2O is approximately in phase in the two hemispheres. In NH winter/spring, air entering DT regions of both hemispheres near the height of Tp2 is drier than that of ST regions, and in NH summer it is wetter; in both cases in mixed H_2O is in phase with the seasonal varying temperature of the tropical Lagrangian cold point [e.g., *Hoor et al.*, 2010] that controls humidity at the base of the TTL. Furthermore, the slow ascent of this tropical signal in the tropical H_2O "tape recorder" [*Mote et al.*, 1996] is also imprinted in extratropical DT-ST% in the first ∼10 km above Tp1 from both instruments. These upward propagating extratropical anomalies are almost certainly not due to wide-scale slow ascent in the extratropical lower stratosphere, a region generally dominated by the slow descent of the lower branch of the BDC. Rather, they more likely result from rapid quasi-isentropic transport from the TTL into the midlatitude LMS [e.g., in Rossby wave breaking events that transport material from the tropics to midlatitudes on timescales of a few days, *Homeyer and Bowman*, 2013]. While *Homeyer et al.* [2014] found a significant relationship between DT regions and convective injection of H_2O into the stratosphere, suggesting that both vertical transport of tropospheric air into DT regions can be a source of enhanced H_2O, the "imprint" of the tape recorder on the DT-ST% column is strong evidence that horizontal transport into the DT layer from the TTL is an important mechanism for DT trace gas variations.

Figure 11 (bottom) shows that January–February H_2O DT-ST 4 km above Tp1 is generally negative but has positive values in the NH along the edge of the tropics in the western Pacific (90°E–165°W). While DT parcels in this region are drier than ST parcels in their median, there is a population of very wet outliers among the DT cases, with H_2O mixing ratios at times exceeding 100 ppmv (not shown) that pulls the DT mean 0.8 ppmv above the median at these longitudes, at latitudes between the STJ and 40°N. The provenance of these wet parcels that have avoided the dehydration in the TTL will be a subject of further investigation.

The broad agreement in H_2O between MLS and HIRDLS suggests that the HIRDLS H_2O product (which is new in v7 and thus has not been extensively validated) is, indeed, capturing the large-scale variations in H_2O. MLS DT-ST H_2O differences are almost unchanged when MLS data are limited to the HIRDLS time period (not shown), so differences in detail (e.g., the weaker HIRDLS DT-ST negative anomaly) are not the result of the years sampled by the two instruments but may result from slightly different latitudinal sampling, artifacts in the HIRDLS H_2O, and/or the differences in vertical resolution of the two instruments.

3.2.5. Carbon Monoxide

Figure 14 shows MLS and ACE-FTS CO mean climatologies (first and second columns) and DT-ST climatologies (third and fourth columns). Here DT-ST (mixing ratio difference) plots are shown rather than DT-ST% (percentage difference) plots to avoid overemphasizing small, higher altitude differences when the denominator of DT-ST% is small. In the ~10 km above Tp1, the MLS mean CO profile does not drop off as rapidly as is expected given its lifetime in the stratosphere and as is seen in the ACE-FTS mean CO profile. MLS mean CO exhibits a strong seasonal cycle 3–7 km above Tp1, which is similar in form to the DT-ST signatures in ACE-FTS, indicating that MLS sees higher CO in the seasons where ACE-FTS sees its largest DT-ST differences, yet this seasonal increase in MLS CO is not well correlated with the presence of DTs and so is not reflected in the MLS DT-ST plot. Recent validation work (M. I. Hegglin et al., SPARC Data Initiative: Comparison of trace gas and aerosol climatologies from international satellite limb sounders, manuscript in preparation, 2015) suggests that MLS CO has unexpectedly weak equator-to-pole gradients and is biased high in the lower stratosphere; the lack of expected signatures in MLS CO in the context of double tropopauses may be related to such biases. While ACE-FTS products generally suffer from its sparse sampling, the signatures seen in its DT-ST CO plots are generally consistent with those expected of a tropospheric tracer with CO's lifetime, with elevated DT-ST values of 6–7 ppbv at and just below Tp2, mirroring (with opposite sign) those seen in the DT-ST% plots of the stratospheric tracers. Analysis repeated in narrow latitudinal bands (not shown) suggests that the poleward biased latitudinal sampling of ACE-FTS is not the source of differences between the observations from the two instruments.

3.2.6. Other Tracers

In addition to the trace gases discussed above, MLS, HIRDLS, and ACE-FTS measure several other tropospheric tracers (not shown) that provide information on transport in the UTLS. Examination of several of these products (e.g., ACE-FTS CH_4 and CH_3Cl and CFC-11 and CFC-12 from both ACE-FTS and HIRDLS) reveals patterns that are roughly consistent with those shown above. HIRDLS CFC-11 and CFC-12 have March–April peaks of 18 pptv (9%) and 24 pptv (5%), respectively, at the level of Tp2 that are approximately in phase (with the sign reversed) with those in the stratospheric tracers. These results are also consistent (within the sampling limitations) with ACE-FTS CO and with the lateral propagation of the tape recorder signal seen in H_2O (which could result only from horizontal transport from the tropics). The consistency of numerous tracers, both stratospheric and tropospheric, with differing vertical and horizontal gradients and tropical tropopause-level sources/sinks, offers strong evidence that transport from the TTL is an important factor in determining the trace gas distributions in DT regions.

4. Summary and Conclusions

UTLS measurements from three satellite instruments are used to examine in detail the distributions of multiple trace gases in regions with extratropical double versus single tropopauses. Data from Aura MLS for 2005–2012, Aura HIRDLS for 2005–2007, and ACE-FTS for 2005–2010 are analyzed and compared. The use of multiple trace gases from three instruments with very different measurement approaches provides a consistency test of the derived results. This work constitutes the first comprehensive multiyear, multispecies climatology of trace gas signatures associated with the presence of double tropopauses and also provides information on interinstrument consistency and sampling issues. Results from the three instruments are generally consistent. MLS provides the longest data record with good latitudinal coverage so would generally be preferred for species it retrieves if a single data set had to be chosen. ACE-FTS and HIRDLS have somewhat better vertical resolution and provide additional species that confirm results, albeit with the limited geographic and temporal sampling of ACE-FTS and the limited years of coverage and problematic measurement system of HIRDLS.

The presence of low sPV and N^2 (from GEOS-5 data) ~2–8 km above the primary tropopause (Tp1) in double-tropopause (DT) regions is consistent with the premise that air has entered this layer above the extratropical tropopause inversion layer (TIL) from the tropical tropopause layer (TTL), consistent with

previous work [e.g., *Homeyer and Bowman*, 2013; *Pan et al.*, 2009]. We show here that this premise is consistent with increases in tropospheric tracers and decreases in stratospheric tracers in this layer. As has been shown in previous studies [*Manney et al.*, 2014, and references therein], DTs are more common in winter than in summer and in the NH than in the SH. Winter-spring DT occurrence maxima are found in the NH in regions with climatologically strong STJs and in summer poleward of the Asian and North American monsoons. Longitudinal variations in the SH are weaker. These climatological differences in distributions and dynamical characteristics of DTs and STs are associated with distinct differences in trace gas distributions.

The stratospheric tracers O_3, HNO_3, and HCl have lower values in DT than in ST regions ~2–8 km above Tp1 in all seasons. The largest differences are in winter in the NH, with maximum differences near 50% (slightly more for O_3 and HNO_3 and slightly less for HCl); NH summertime differences near 20–35% coincide with a lower frequency of DTs and with a Tp2 that is about 1 km closer in altitude to Tp1 (resulting from a slight rising of Tp1 and a slight lowering of Tp2). In the SH, wintertime differences are lower by ~10–15% than those in the NH, while summertime differences are similar between the hemispheres. Very similar results are seen for O_3 and HNO_3, with small differences between MLS and HIRDLS fields attributable to the different time periods sampled, but with no indication that the coarser MLS vertical resolution leads to biases. DT signatures in stratospheric tracers from ACE-FTS are broadly consistent with those from MLS and HIRDLS but have biases resulting from the sparse and irregular ACE-FTS sampling with respect to the seasonal cycle. In particular, in November through February in the NH, and May through August in the SH, the ACE-FTS sampling is strongly biased toward higher latitudes, resulting in a smaller fraction of DTs, and higher Tp2 altitudes. These sampling limitations result in larger DT-ST differences in ACE-FTS at higher altitudes and the appearance of discontinuities in the seasonal evolution of DT-ST trace gas differences.

The seasonal cycles in H_2O anomalies associated with DT regions in both hemispheres are controlled by the seasonal cycle in H_2O near the tropical tropopause. This tropical cycle includes effects of seasonal changes in the temperature of the tropical Lagrangian cold trap as well as the large influx of moisture from the Asian summer monsoon. DTs are associated with strong negative (positive) H_2O anomalies in both hemispheres in November through February (July through October) and weaker differences in the intervening seasons. DT-ST H_2O anomalies propagate upward in time, in phase with the tropical H_2O tape recorder. This pattern is not the result of local slow ascent but rather is more likely the result of fast, quasi-isentropic transport copying the tropical tape recorder signal into the extratropics.

As is the case with stratospheric tracers, the magnitude of DT-ST H_2O differences is smaller in the SH than in the NH, with maximum DT-ST magnitudes near 15% (10%) in the NH (SH). H_2O exhibits extremely strong gradients across the tropopause, making retrievals from satellite data in this region difficult and resolution dependent, so it is not unexpected that the newly available HIRDLS H_2O product does not agree quite as well with MLS H_2O as do the MLS and HIRDLS O_3 and HNO_3 products. Broad agreement in the MLS and HIRDLS H_2O distributions near the tropopauses supports the scientific utility of HIRDLS H_2O. However, higher in the stratosphere, HIRDLS H_2O mixing ratios do not increase with height as would be expected from methane oxidation and as do MLS values.

Total MLS extratropical CO has higher values 2–10 km above Tp1 and a larger winter-peaking seasonal cycle than does total ACE-FTS CO, but the winter peak in MLS CO is not well correlated with the presence of DTs and so does not result in a prominent corresponding peak in the MLS DT-ST CO. ACE-FTS, despite its poorer temporal and latitudinal sampling, does display a peak in CO DT-ST at and just below the level of Tp2 in the DT profiles, roughly mirroring the DT-ST% minimum seen in stratospheric tracers such as O_3 from MLS and HIRDLS and more closely mirroring the patterns of ACE-FTS O_3 DT-ST% (not shown), which shares its sampling. As with the stratospheric tracers, this peak is stronger in winter/spring than in summer/fall, consistent with the injection of tropospheric tracers and dilution of stratospheric tracers in this layer of the DT profiles by common dynamics.

Large differences in trace gas distributions between DT and ST regions that are consistent among three satellite data sets and across numerous trace gases show distinct signatures of air from the TTL region, providing strong evidence that transport from this region is an important pathway for troposphere-to-stratosphere exchange related to double tropopauses. The magnitude of the DT-ST differences, coupled with the sampled frequency of DT versus ST occurrence, implies that the observed trace gas climatologies in latitude regions where extratropical DTs are common differ by up to ~20% (~10%) in NH (SH) winter from what would be seen in the absence of DTs, with the largest signatures being decreases of this magnitude in

O_3 and HNO_3 in winter. These results, and the availability and consistency of data sets from multiple satellite instruments that provide global multiannual coverage of the UTLS, not only pave the way for future studies using transport calculations to further quantify the roles of different pathways for STE but also provide important climatological information that can be used in assessment of climate models and in studies of the radiative effects of trace gases near the tropopause.

References

Añel, J. A., J. C. Antuña, L. Torre, R. Nieto, and L. Gimeno (2007), Global statistics of multiple tropopauses from the IGRA database, *Geophys. Res. Lett.*, *34*, L06709, doi:10.1029/2006GL029224.

Añel, J. A., J. C. Antuña, L. Torre, and J. M. Castanheira (2008), Climatological features of global multiple tropopause events, *J. Geophys. Res.*, *113*, D00B08, doi:10.1029/2007JD009697.

Añel, J. A., L. Torre, and L. Gimeno (2012), On the origin of the air between multiple tropopauses at midlatitudes, *Sci. World J.*, *2012*, 191028, doi:10.1100/2012/191028.

Bernath, P. F., et al. (2005), Atmospheric Chemistry Experiment (ACE): Mission overview, *Geophys. Res. Lett.*, *32*, L15S01, doi:10.1029/2005GL022386.

Bethan, S., G. Vaughan, and S. J. Reid (1996), A comparison of ozone and thermal tropopause heights and the impact of tropopause definition on quantifying the ozone content of the troposphere, *Q. J. R. Meteorolog. Soc.*, *122*, 929–944.

Birner, T., D. Sankey, and T. Shepherd (2006), The tropopause inversion layer in models and analyses, *Geophys. Res. Lett.*, *33*, L14804, doi:10.1029/2006GL026549.

Bjerknes, J., and E. Palmen (1937), *Investigation of Selected European Cyclones by Means of Serial Ascents*, vol. 12, 62 pp., Am. Meteorol. Soc., Boston, Mass.

Boone, C., R. Nassar, K. Walker, Y. Rochon, S. McLeod, C. Rinsland, and P. Bernath (2005), Retrievals for the atmospheric chemistry experiment Fourier-transform spectrometer, *Appl. Opt.*, *44*(33), 7218–7231.

Boone, C., K. Walker, and P. Bernath (2013), Version 3 retrievals for the Atmospheric Chemistry Experiment Fourier Transform Spectrometer (ACE-FTS), in *The Atmospheric Chemistry Experiment ACE at 10: A Solar Occultation Anthology*, edited by P. Bernath, pp. 103–127, A. Deepak, Hampton, Va. [Available at http://www.ace.uwaterloo.ca/publications.html#ValidationPapers.]

Castanheira, J. M., J. A. Añel, C. A. F. Marques, J. C. Antuña, M. L. R. Liberato, L. de la Torre, and L. Gimeno (2009), Increase of upper troposphere/lower stratosphere wave baroclinicity during the second half of the 20th century, *Atmos. Chem. Phys.*, *9*, 9143–9153, doi:10.5194/acp-9-9143-2009.

Castanheira, J. M., T. R. Peevey, C. A. Marques, and M. A. Olsen (2012), Relationships between Brewer-Dobson circulation, double tropopauses, ozone and stratospheric water vapour, *Atmos. Chem. Phys.*, *12*(21), 10,195–10,208, doi:10.5194/acp-12-10195-2012.

Clerbaux, C., et al. (2008), CO measurements from the ACE-FTS satellite instrument: Data analysis and validation using ground-based, airborne and spaceborne observations, *Atmos. Chem. Phys.*, *8*, 2569–2594, doi:10.5194/acp-8-2569-2008.

Danielsen, E. F. (1968), Stratospheric-tropospheric exchange based on radioactivity, ozone and potential vorticity, *J. Atmos. Sci.*, *25*, 502–518.

Duncan, B. N., S. E. Strahan, Y. Yoshida, S. D. Steenrod, and N. Livesey (2007), Model study of the cross-tropopause transport of biomass burning pollution, *Atmos. Chem. Phys.*, *7*, 3713–3736.

Dunkerton, T. J., and D. P. Delisi (1986), Evolution of potential vorticity in the winter stratosphere of January–February 1979, *J. Geophys. Res.*, *91*, 1199–1208.

Dupuy, E., et al. (2009), Validation of ozone measurements from the Atmospheric Chemistry Experiment (ACE), *Atmos. Chem. Phys.*, *9*, 287–343.

Ertel, H. (1942), Ein neuer hydrodynamischer Wirbelsatz, *Meteorol. Z.*, *59*(9), 277–281.

Forster, P. M., and K. P. Shine (1997), Radiative forcing and temperature trends from stratospheric ozone changes, *J. Geophys. Res.*, *102*, 10,841–10,855.

Froidevaux, L., et al. (2008), Validation of Aura Microwave Limb Sounder HCl measurements, *J. Geophys. Res.*, *113*, D15S25, doi:10.1029/2007JD009025.

Fueglistaler, S., A. Dessler, T. Dunkerton, I. Folkins, Q. Fu, and P. W. Mote (2009), Tropical tropopause layer, *Rev. Geophys.*, *47*, RG1004, doi:10.1029/2008RG000267.

Gettelman, A., P. Hoor, L. L. Pan, W. J. Randel, M. I. Hegglin, and T. Birner (2011), The extratropical upper troposphere and lower stratosphere, *Rev. Geophys.*, *49*, RG3003, doi:10.1029/2011RG000355.

Gille, J., and L. Gray (2013), High Resolution Dynamics Limb Sounder Earth Observing System (EOS) data description and quality version 7 (v7) (HIRDLS version 7.00.00), *Tech. Rep. SC-HIR-1511K*, Oxford Univ., Univ. of Colo., Nat'l. Cent. for Atmos. Res. [Available at http://www.eos.ucar.edu/hirdls/data/products/HIRDLS-DQD_V7-1.pdf.]

Gille, J., J. Barnett, J. Whitney, M. Dials, D. Woodard, W. Rudolf, A. Lambert, and W. Mankin (2003), The High-Resolution Dynamics Limb Sounder (HIRDLS) experiment on Aura, in *Proceedings of SPIE, Infrared Spaceborne Remote Sensing XI*, vol. 5152, edited by Marija Strojnik, 162 pp., San Diego, Calif.

Gille, J., et al. (2005), Development of special corrective processing of HIRDLS data and early validation, in *Proceedings of SPIE, Infrared Spaceborne Remote Sensing 2005*, vol. 5883, edited by Marija Strojnik, p. 58830H, San Diego, Calif.

Grise, K. M., D. W. Thompson, and T. Birner (2010), A global survey of static stability in the stratosphere and upper troposphere, *J. Clim.*, *23*(9), 2275–2292.

Grise, K. M., L. M. Polvani, G. Tselioudis, Y. Wu, and M. D. Zelinka (2013), The ozone hole indirect effect: Cloud-radiative anomalies accompanying the poleward shift of the eddy-driven jet in the Southern Hemisphere, *Geophys. Res. Lett.*, *40*, 3688–3692, doi:10.1002/grl.50675.

Hegglin, M. I., C. D. Boone, G. L. Manney, T. G. Shepherd, K. A. Walker, P. F. Bernath, W. H. Daffer, P. Hoor, and C. Schiller (2008), Validation of ACE-FTS satellite data in the upper troposphere/lower stratosphere (UTLS) using non-coincident measurements, *Atmos. Chem. Phys.*, *8*, 1483–1499.

Hegglin, M. I., C. D. Boone, G. L. Manney, and K. A. Walker (2009), A global view of the extratropical tropopause transition layer (ExTL) from Atmospheric Chemistry Experiment Fourier Transform Spectrometer O_3, H_2O, and CO, *J. Geophys. Res.*, *114*, D00B11, doi:10.1029/2008JD009984.

Hegglin, M. I., et al. (2013), SPARC Data Initiative: Comparison of water vapour climatologies from international satellite limb sounders, *J. Geophys. Res. Atmos.*, *118*, 11,824–11,846, doi:10.1002/jgrd.50752.

Highwood, E. J., B. J. Hoskins, and P. Berrisford (2000), Properties of the Arctic tropopause, *Q. J. R. Meteorol. Soc.*, *126*, 1515–1532.

Hoinka, K. P. (1998), Statistics of the global tropopause pressure, *Mon. Weather Rev.*, *126*(12), 3303–3325, doi:10.1175/1520-0493(1998).

Holton, J. R., P. H. Haynes, M. E. McIntyre, A. R. Douglass, R. B. Rood, and L. Pfister (1995), Stratosphere-troposphere exchange, *Rev. Geophys.*, *33*, 403–439.

Homeyer, C. R., and K. P. Bowman (2013), Rossby wave breaking and transport between the tropics and extratropics above the subtropical jet, *J. Atmos. Sci.*, *70*, 607–626.

Homeyer, C. R., K. P. Bowman, L. L. Pan, E. L. Atlas, R.-S. Gao, and T. L. Campos (2011), Dynamical and chemical characteristics of tropospheric intrusions observed during START08, *J. Geophys. Res.*, *116*, D06111, doi:10.1029/2010JD015098.

Homeyer, C. R., et al. (2014), Convective transport of water vapor into the lower stratosphere observed during double tropopause events, *J. Geophys. Res. Atmos.*, *119*, 10,941–10,958, doi:10.1002/2014JD021485.

Hoor, P., H. Wernli, M. I. Hegglin, and H. Bönisch (2010), Transport timescales and tracer properties in the extratropical UTLS, *Atmos. Chem. Phys.*, *10*(16), 7929–7944, doi:10.5194/acp-10-7929-2010.

Hoskins, B. J., M. E. McIntyre, and A. W. Robertson (1985), On the use and significance of isentropic potential-vorticity maps, *Q. J. R. Meteorol. Soc.*, *111*, 877–946.

Jiang, J. H., N. J. Livesey, H. Su, L. Neary, J. C. McConnell, and N. A. Richards (2007), Connecting surface emissions, convective uplifting, and long-range transport of carbon monoxide in the upper troposphere: New observations from the Aura Microwave Limb Sounder, *Geophys. Res. Lett.*, *34*, L18812, doi:10.1029/2007GL030638.

Jones, R., J. Pyle, J. Harries, A. Zavody, J. Russell, and J. Gille (1986), The water vapour budget of the stratosphere studied using LIMS and SAMS satellite data, *Q. J. R. Meteorol. Soc.*, *112*(474), 1127–1143, doi:10.1002/qj.49711247412.

Kerzenmacher, T. E., et al. (2005), Measurements of O_3, NO_2 and temperature during the 2004 Canadian Arctic ACE validation campaign, *Geophys. Res. Lett.*, *32*, L16S07, doi:10.1029/2005GL023032.

Kinnison, D., et al. (2008), Global observations of HNO_3 from the High Resolution Dynamics Limb Sounder (HIRDLS)—First results, *J. Geophys. Res.*, *113*, D16S42, doi:10.1029/2007JD008833.

Ko, M. K. W., P. A. Newman, and S. E. Strahan (2013), Lifetimes of stratospheric ozone-depleting substances, their replacements, and related species, *SPARC Rep. 6, WCRP-15/2013*, Stratosphere-Troposphere Processes and Their Role in Climate, World Climate Research Program.

Kochanski, A. (1955), Cross sections of the mean zonal flow and temperature along 80°w, *J. Meteorol.*, *12*, 95–106, doi:10.1175/1520-0469(1955)012.

Krebsbach, M., C. Schiller, D. Brunner, G. Günther, M. Hegglin, D. Mottaghy, M. Riese, N. Spelten, and H. Wernli (2006), Seasonal cycles and variability of O_3 and H_2O in the UT/LMS during SPURT, *Atmos. Chem. Phys.*, *6*(1), 109–125, doi:10.5194/acp-6-109-2006.

Kunz, A., P. Konopka, R. Müller, and L. L. Pan (2011), Dynamical tropopause based on isentropic potential vorticity gradients, *J. Geophys. Res.*, *116*, D01110, doi:10.1029/2010JD014343.

Livesey, N. J., et al. (2008), Validation of Aura Microwave Limb Sounder O_3 and CO observations in the upper troposphere and lower stratosphere, *J. Geophys. Res.*, *113*, D15S02, doi:10.1029/2007JD008805.

Livesey, N. J., et al. (2013), Version 3.3 and 3.4 Level 2 data quality and description document, *Tech. Rep. JPL D-33509*, Jet Propulsion Laboratory, Pasadena, Calif. [Available at http://mls.jpl.nasa.gov.]

Lorenz, D. J., and E. T. DeWeaver (2007), Tropopause height and zonal wind response to global warming in the IPCC scenario integrations, *J. Geophys. Res.*, *112*, D10119, doi:10.1029/2006JD008087.

Mahieu, E., et al. (2008), Validation of ACE-FTS v2.2 measurements of HCl, HF, CCl_3F and CCl_2F_2 using space-, balloon- and ground-based instrument observations, *Atmos. Chem. Phys.*, *8*(20), 6199–6221.

Manney, G. L., R. W. Zurek, A. O'Neill, and R. Swinbank (1994), On the motion of air through the stratospheric polar vortex, *J. Atmos. Sci.*, *51*, 2973–2994.

Manney, G. L., et al. (2007), Solar occultation satellite data and derived meteorological products: Sampling issues and comparisons with Aura Microwave Limb Sounder, *J. Geophys. Res.*, *112*, D24S50, doi:10.1029/2007JD008709.

Manney, G. L., et al. (2009), Satellite observations and modelling of transport in the upper troposphere through the lower mesosphere during the 2006 major stratospheric sudden warming, *Atmos. Chem. Phys.*, *9*, 4775–4795.

Manney, G. L., et al. (2011), Jet characterization in the upper troposphere/lower stratosphere (UTLS): Applications to climatology and transport studies, *Atmos. Chem. Phys.*, *11*(12), 6115–6137.

Manney, G. L., M. I. Hegglin, W. H. Daffer, M. J. Schwartz, M. L. Santee, and S. Pawson (2014), Climatology of upper tropospheric/lower stratospheric (UTLS) jets and tropopauses in MERRA, *J. Clim.*, *27*(9), 3248–3271, doi:10.1175/JCLI-D-13-00243.1.

Martius, O., L. M. Polvani, and H. C. Davies (2009), Blocking precursors to stratospheric sudden warming events, *Geophys. Res. Lett.*, *36*, L14806, doi:10.1029/2009GL038776.

McLandress, C., T. G. Shepherd, J. F. Scinocca, D. A. Plummer, M. Sigmond, A. I. Jonsson, and M. C. Reader (2011), Separating the dynamical effects of climate change and ozone depletion. Part II: Southern Hemisphere troposphere, *J. Clim.*, *24*, 1850–1868, doi:10.1175/2010JCLI3958.1.

Mote, P. W., K. H. Rosenlof, M. E. McIntyre, E. S. Carr, J. C. Gille, J. R. Holton, J. S. Kinnersley, H. C. Pumphrey, J. M. Russell III, and J. W. Waters (1996), An atmospheric tape recorder: The imprint of tropical tropopause temperatures on stratospheric water vapor, *J. Geophys. Res.*, *101*, 3989–4006.

Nakamura, N. (2007), Extratropical stratosphere-troposphere mass exchange associated with isentropic mixing: A 1992–2005 climatology derived from advection-diffusion calculations, *J. Geophys. Res.*, *112*, D24303, doi:10.1029/2006JD008382.

Nardi, B., et al. (2008), Initial validation of ozone measurements from the High Resolution Dynamics Limb Sounder, *J. Geophys. Res.*, *113*, D16S36, doi:10.1029/2007JD008837.

Pan, L., W. Randel, J. Gille, W. D. Hall, B. Nardi, S. Massie, V. Yudin, R. Khosravi, P. Konopka, and D. Tarasick (2009), Tropospheric intrusions associated with the secondary tropopause, *J. Geophys. Res.*, *114*, D10302, doi:10.1029/2008JD011374.

Pan, L. L., W. J. Randel, B. L. Gary, M. J. Mahoney, and E. J. Hintsa (2004), Definitions and sharpness of the extratropical tropopause: A trace gas perspective, *J. Geophys. Res.*, *109*, D23103, doi:10.1029/2004JD004982.

Pan, L. L., P. Konopka, and E. V. Browell (2006), Observations and model simulations of mixing near the extratropical tropopause, *J. Geophys. Res.*, *111*, D05106, doi:10.1029/2005JD006480.

Peevey, T., J. Gille, C. Homeyer, and G. Manney (2014), The double tropopause and its dynamical relationship to the tropopause inversion layer in storm track regions, *J. Geophys. Res. Atmos.*, *119*, 10,194–10,212, doi:10.1002/2014JD021808.

Peevey, T. R., J. C. Gille, C. E. Randall, and A. Kunz (2012), Investigation of double tropopause spatial and temporal global variability utilizing High Resolution Dynamics Limb Sounder temperature observations, *J. Geophys. Res.*, *117*, D01105, doi:10.1029/2011JD016443.

Randel, W. J., and F. Wu (2010), The polar summer tropopause inversion layer, *J. Atmos. Sci.*, *67*, 2572–2581, doi:10.1175/2010JAS3430.1.

Randel, W. J., D. J. Seidel, and L. Pan (2007a), Observational characteristics of double tropopauses, *J. Geophys. Res.*, *112*, D07309, doi:10.1029/2007JD007904.

Randel, W. J., F. Wu, and P. Forster (2007b), The extratropical tropopause inversion layer: Global observations with GPS data, and a radiative forcing mechanism, *J. Atmos. Sci.*, *64*(12), 4489–4496, doi:10.1175/2007JAS2412.1.

Read, W. G., et al. (2007), Aura Microwave Limb Sounder upper tropospheric and lower stratospheric H_2O and relative humidity with respect to validation, *J. Geophys. Res.*, *112*, D24S35, doi:10.1029/2007JD008752.

Rienecker, M. M., et al. (2008), The GEOS-5 data assimilation system—Documentation of versions 5.0.1, 5.1.0, and 5.2.0, *Tech. Rep. TM-2008-104606*, NASA, Goddard Space Flight Center, Greenbelt, Md.

Santee, M. L., et al. (2007), Validation of the Aura Microwave Limb Sounder HNO_3 measurements, *J. Geophys. Res.*, *112*, D24S40, doi:10.1029/2007JD008721.

Santee, M. L., G. L. Manney, L. Froidevaux, N. J. Livesey, W. G. Read, and M. J. Schwartz (2011), Trace gas evolution in the lowermost stratosphere from Aura Microwave Limb Sounder measurements, *J. Geophys. Res.*, *116*, D18306, doi:10.1029/2011JD015590.

Schiemann, R., D. Lüthi, and C. Schar (2009), Seasonality and interannual variability of the westerly jet in the Tibetan Plateau region, *J. Clim.*, *22*, 2940–2957, doi:10.1175/2008JCLI2625.1.

Schmidt, T., G. Beyerle, S. Heise, J. Wickert, and M. Rothacher (2006), A climatology of multiple tropopauses derived from GPS radio occultations with CHAMP and SAC-C, *Geophys. Res. Lett.*, *33*, L04808, doi:10.1029/2005GL024600.

Schoeberl, M. R. (2004), Extratropical stratosphere-troposphere mass exchange, *J. Geophys. Res.*, *109*, D13303, doi:10.1029/2004JD004525.

Schwartz, M. J., W. G. Read, M. L. Santee, N. J. Livesey, L. Froidevaux, A. Lambert, and G. L. Manney (2013), Convectively injected water vapor in the North American summer lowermost stratosphere, *Geophys. Res. Lett.*, *40*, 2316–2321, doi:10.1002/grl.50421.

Seidel, D. J., and W. J. Randel (2006), Variability and trends in the global tropopause estimated from radiosonde data, *J. Geophys. Res.*, *111*, D21101, doi:10.1029/2006JD007363.

Shapiro, M. A. (1980), Turbulent mixing within tropopause folds as a mechanism for the exchange of chemical constituents between the stratosphere and troposphere, *J. Atmos. Sci.*, *37*, 994–1004.

Shepherd, T. G. (2002), Issues in stratosphere-troposphere coupling, *J. Meteorol. Soc. Jpn.*, *80*, 769–792.

Shuckburgh, E., F. d'Ovidio, and B. Legras (2009), Local mixing events in the upper troposphere and lower stratosphere. Part II: Seasonal and interannual variability, *J. Atmos. Sci.*, *66*, 3695–3706.

Solomon, S., K. H. Rosenlof, R. W. Portmann, J. S. Daniel, S. M. Davis, T. J. Sanford, and G.-K. Plattner (2010), Contributions of stratospheric water vapor to decadal changes in the rate of global warming, *Science*, *327*, 1219–1223.

Son, S., L. M. Polvani, D. W. Waugh, H. Akiyoshi, R. Garcia, D. Kinnison, S. Pawson, E. Rozanov, T. G. Shepherd, and K. Shibata (2008), The impact of stratospheric ozone recovery on the Southern Hemisphere westerly jet, *Science*, *320*, 1486–1489.

Stohl, A., et al. (2003), Stratosphere-troposphere exchange: A review, and what we have learned from STACCATO, *J. Geophys. Res.*, *108*(D12), 8516, doi:10.1029/2002JD002490.

Ungermann, J., et al. (2013), Filamentary structure in chemical tracer distributions near the subtropical jet following a wave breaking event, *Atmos. Chem. Phys.*, *13*, 10,517–10,534.

Vogel, B., et al. (2011), Transport pathways and signatures of mixing in the extratropical tropopause region derived from Lagrangian model simulations, *J. Geophys. Res.*, *116*, D05306, doi:10.1029/2010JD014876.

Vömel, H., D. David, and K. Smith (2007), Accuracy of tropospheric and stratospheric water vapor measurements by the cryogenic frost point hygrometer: Instrumental details and observations, *J. Geophys. Res.*, *112*, D08305, doi:10.1029/2006JD007224.

Wang, S., and L. M. Polvani (2011), Double tropopause formation in idealized baroclinic life cycles: The key role of an initial tropopause inversion layer, *J. Geophys. Res.*, *116*, D05108, doi:10.1029/2010JD015118.

Waters, J. W., et al. (2006), The Earth Observing System Microwave Limb Sounder (EOS MLS) on the Aura satellite, *IEEE Trans. Geosci. Remote Sens.*, *44*, 1075–1092.

Wilcox, L. J., B. J. Hoskins, and K. P. Shine (2012), A global blended tropopause based on ERA data. Part I: Climatology, *Q. J. R. Meteorol. Soc.*, *138*, 561–575.

Wolff, M., et al. (2008), Validation of HNO_3, $ClONO_2$, and N_2O_5 from the Atmospheric Chemistry Experiment Fourier Transform Spectrometer (ACE-FTS), *Atmos. Chem. Phys.*, *8*(13), 3529–3562.

Woollings, T., A. Hannachi, and B. Hoskins (2010a), Variability of the North Atlantic eddy-driven jet stream, *Q. J. R. Meteorol. Soc.*, *136*, 856–868.

Woollings, T., A. Charlton-Perez, S. Ineson, G. Marshall, and G. Masato (2010b), Associations between stratospheric variability and tropospheric blocking, *J. Geophys. Res.*, *115*, D06108, doi:10.1029/2009JD012742.

World Meteorological Organization (1957), Meteorology—A three-dimensional science: Second session of the commission for aerology, *WMO Bull.*, *14*, 134–138.

World Meteorological Organization (2011), Scientific assessment of ozone depletion: 2010, *Global Ozone Res. and Monit. Proj. Rep. 52*, Geneva, Switzerland.

Zängl, G., and K. P. Hoinka (2001), The tropopause in the polar regions, *J. Clim.*, *14*, 3117–3139, doi:10.1175/1520-0442(2001)014.